

Review

Microalloyed Steels through History until 2018: Review of Chemical Composition, Processing and Hydrogen Service

Julio C. Villalobos ¹, Adrian Del-Pozo ², Bernardo Campillo ^{3,4}, Jan Mayen ⁵  and Sergio Serna ^{2,*} 

¹ Instituto Tecnológico de Morelia, Avenida Tecnológico No. 1500, Col. Lomas de Santiaguito, Morelia 58120, México; julio.villalobos@uaem.mx

² CIICAp, Universidad Autónoma del Estado de Morelos, Av. Universidad 1001, Col. Chamilpa, Cuernavaca 62609, Mexico; adrian.delpozo@alumnos.uaem.mx

³ Instituto de Ciencias Físicas-UNAM, Av. Universidad 1001, Col. Chamilpa, Cuernavaca 62609, Mexico; bci@fis.unam.mx

⁴ Facultad de Química-UNAM, Circuito de la Investigación Científica S/N, Mexico City 04510, Mexico

⁵ CONACYT, CIATEQ, Unidad San Luis Potosí, Eje 126 No. 225, Zona Industrial, San Luis Potosí 78395, Mexico; jan.mayen@ciateq.mx

* Correspondence: aserna@uaem.mx; Tel.: +52-777-329-7084

Received: 22 March 2018; Accepted: 25 April 2018; Published: 14 May 2018



Abstract: Microalloyed steels have evolved in terms of their chemical composition, processing, and metallurgical characteristics since the beginning of the 20th century in the function of fabrication costs and mechanical properties required to obtain high-performance materials needed to accommodate for the growing demands of gas and hydrocarbons transport. As a result of this, microalloyed steels present a good combination of high strength and ductility obtained through the addition of microalloying elements, thermomechanical processing, and controlled cooling, processes capable of producing complex microstructures that improve the mechanical properties of steels. These controlled microstructures can be severely affected and result in catastrophic failures, due to the atomic hydrogen diffusion that occurs during the corrosion process of pipeline steel. Recently, a martensite–bainite microstructure with acicular ferrite has been chosen as a viable candidate to be used in environments with the presence of hydrogen. The aim of this review is to summarize the main changes of chemical composition, processing techniques, and the evolution of the mechanical properties throughout recent history on the use of microalloying in high strength low alloy steels, as well as the effects of hydrogen in newly created pipelines, examining the causes behind the mechanisms of hydrogen embrittlement in these steels.

Keywords: microalloyed steels; mechanical properties; processing; microstructural and chemical composition; hydrogen embrittlement

1. Introduction

Steel has represented a great advance in the history of the humanity, due to its multiple uses and excellent properties. Throughout history, great discoveries have been made through the knowledge of the phenomena that dominate the behavior of alloys, such as chemical composition, microstructure and thermomechanical processes. Many researchers have contributed to this knowledge and laid the foundations responsible for the continuous developments in the field of metallurgy.

In the last 50 years, the strength of steels has increased progressively thanks to advances in metallurgy and manufacturing techniques in response to the market demand for lighter and

stronger steels. The need to achieve these characteristics of higher strength and weldability with sufficient toughness and ductility has led to the development of high strength low alloy (HSLA) steels. HSLA steels typically contain very low carbon content and small amounts of alloying elements [1], and these are classified by the American Petroleum Institute (API) in order of its strength (X-42, X-46, X-52, X-56, X-60, X-65, X-70, X-80, X-100 and X-120). These properties are achieved by a careful selection of microalloy composition and optimization of thermomechanical processing (TMP) and accelerated cooling conditions subsequent to the TMP.

HSLA steels have been developed to obtain improved mechanical properties compared to normal carbon steels, as well as superior corrosion resistance properties. Alloying elements include 0.05–0.25% carbon, manganese content up to 2%, and small amounts of chromium, nickel, molybdenum, copper, nitrogen, vanadium, niobium, titanium and zirconium that can be used in different proportions [2].

There are many types of HSLA steels, such as weathering steels, microalloyed ferrite-pearlite steels, as-rolled pearlitic steels, acicular ferrite steels, dual phase steels, and inclusion shape-controlled steels. Commonly weathering steels have compositions that include small quantities of alloying elements to improve corrosion resistance; additions of copper are often used in atmospheres where the levels of phosphorus and sulfur are low in the air. In general, microalloyed ferrite-pearlite steels present compositions with small percentages of carbide formers like vanadium and titanium, which strengthen the steel via precipitation hardening and grain refinement. As-rolled pearlitic steels typically only contain carbon and manganese but can have additions of other elements to increase their strength. Dual phase steels use microalloying to create a ferrite matrix with dispersed martensite [2].

The importance of these steels lies in their use in a wide variety of commercial and industrial applications; as a result of this, they have served as crucial materials to achieve great advances in many fields, such as: construction, heavy duty vehicles, storage tanks, railroad cars, oil rigs, pipes for hydrocarbon transport and many more.

2. Chemical Composition of Microalloyed Steels

High Strength Low Alloy (HSLA) steels were introduced at the beginning of the 20th century and the main elements used in a low wt % combination are Nb, V, and Ti. The microalloyed steels (as later were named) use a small amount of microalloying elements ranging from 0.10 up to 0.15 wt %, for single and multi-elements [3], and are either Nb, V or Ti alloyed [4].

The use of microalloyed elements was first reported in the literature around the years 1938–1939, with the use of Nb as a strengthener of hot rolled C-Mn steels [5]. Subsequently, in the year 1945, the V effects were used to increase the strength of normalized steels, but these new microalloyed steels had low impact toughness and ductility [6,7]. It was well known the advantage of grain refining effects due to precipitation of microalloyed elements in the presence of N and C, promoting the precipitation of carbides, nitrides and carbonitrides (Nb, V) (C, N), but the strengthening mechanism was not clear.

The increase of Mn content has been correlated to a reduction of the harmful effect on toughness caused by the precipitation of V and Nb carbonitrides [8], and it was later discovered that Nb could retard the austenite recrystallization [9], which was the introduction of controlled rolling and thermomechanical controlled processing [10]. Mo and Al were used to retard the austenite recrystallization, but it was determined that Nb was the most effective [11]. Later, the use of other elements Zr, B and rare earth metals were used for the control of inclusions, and the controlled additions of S were added to improve the machinability [12]. The effect of microalloying content (wt %) on austenite recrystallization is shown in Figure 1.

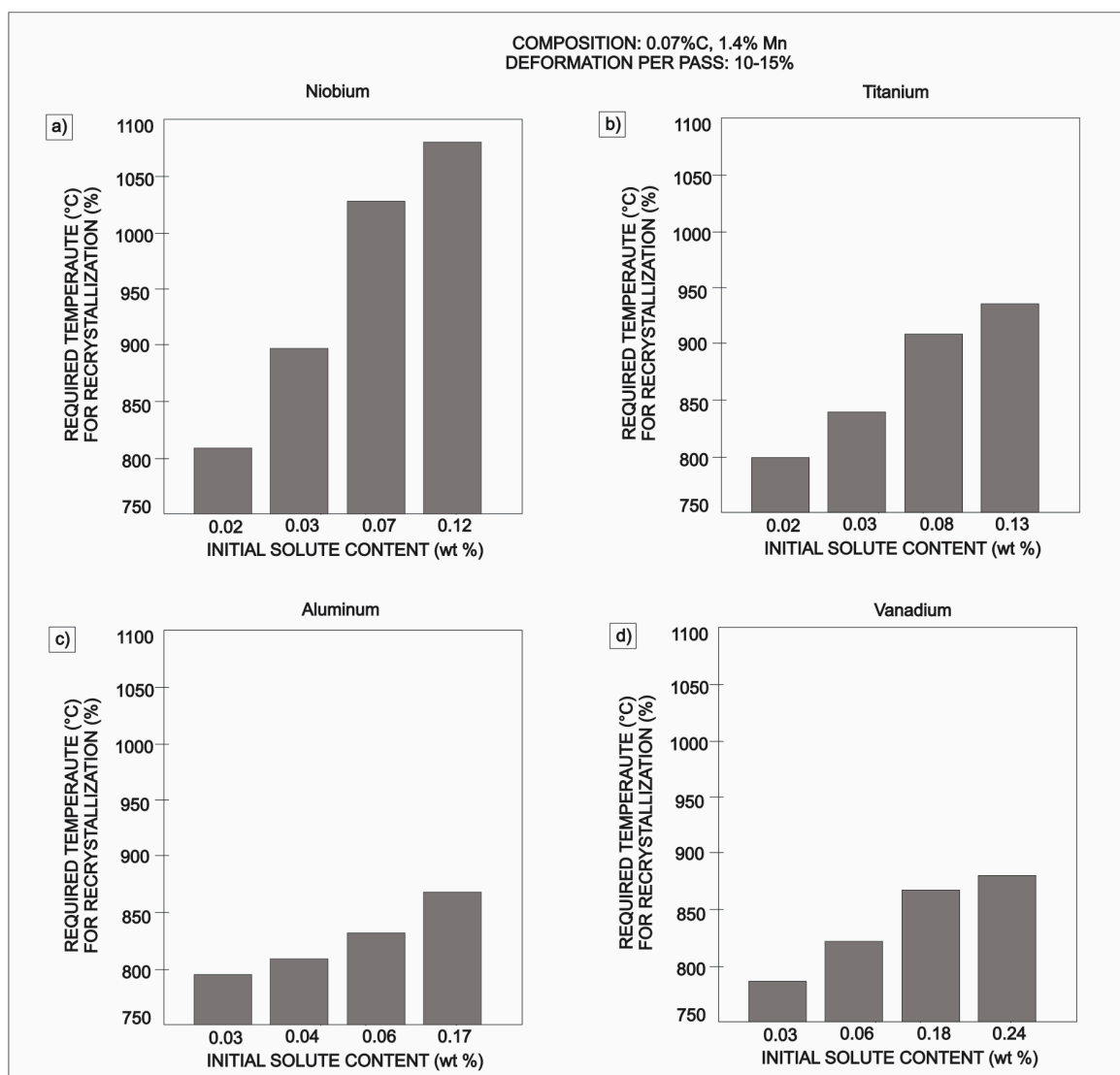


Figure 1. Austenite recrystallization as a function of microalloying content, (a) niobium, (b) titanium, (c) aluminum and (d) vanadium, content [12].

The early work on Nb microalloyed steels was concentrated in the USA and UK; in the year 1958, the American company National Steel Corporation developed an Nb-treated steel with relatively low cost with the addition of 0.005–0.03% of Nb content, obtaining a combined effect on strengthening and good toughness [13], this semikilled C-Mn steel is able to achieve a yield strength in a range of 300 up to 415 MPa. Furthermore, V was used in combination of Cr-Mo to improve the creep resistance at high temperatures, which was attributed to their high temperature stability [14], with a maximum working temperature of 400 °C.

In the 1970s, the strengthening mechanism was developed by the optimization of chemical composition and processing. The principal mechanisms that even modern high strength steels still use are grain size refinement, solid solution by Mn, Mo, Si, Cu, Ni, Cr addition, precipitation hardening due to the formation of Nb, V, Ti carbonitrides, increased dislocation density and fine grain microstructure generated by a thermomechanical controlled processing and controlled cooling that enhance the mechanical properties [15–17], and decreases the transformation temperature. In accordance with Vervynck et al. [18], the solid solution strengthening is directly related to the microalloyed content, while grain size refinement and precipitation hardening is a function of the interaction between microalloying elements and strain percent during thermomechanical controlled processes (TMCPs).

The C content used in HSLA steels before 1980 was 0.07–0.12%; meanwhile, up to 2% of Mn content was commonly employed together with different additions and combinations of V, Nb and Ti (max. 0.1%) [19]. Reducing the C content could improve the weldability maintaining strength, and it was equal to mild steels, but the principal problem of reducing the C content was that ductility and toughness were not as good as quenched and tempered steels [19].

Controlling the critical temperatures of austenite, microalloying elements can be adjusted to achieve the final mechanical properties required for some applications. These critical temperatures are: the grain coarsening temperature during reheating, recrystallization temperature during hot rolling and transformation temperature during cooling [20,21]. The principal effects of microalloying elements are summarized in Table 1.

Table 1. Principal effect of microalloyed elements [18].

Element	wt %	Effect
C	<0.25	Strengthener
Mn	0.5–2.0	Retards the austenite decomposition during accelerated cooling Decreases ductile to brittle transitions temperature Strong sulfide former
Si	0.1–0.5	Deoxidizer in molten steel Solid solution strengthener
Al	<0.02	Deoxidizer Limits grain growths as aluminum nitride
Nb	0.02–0.06	Very strong ferrite strengthener as niobium carbides/nitrides Delays austenite–ferrite transformation
Ti	0–0.06	Austenite grain control by titanium nitrides Strong ferrite strengthener
V	0–0.10	Strong ferrite strengthener by vanadium carbonitrides
Zr	0.002–0.05	Austenite grain size control Strong sulfide former
N	<0.012	Strong former of nitrides and carbonitrides with microalloyed elements
Mo	0–0.3	Promotes bainite formations Ferrite strengthener
Ni	0–0.5	Increase fracture toughness
Cu	0–0.55	Improves corrosion resistance Ferrite strengthener
Cr	0–1.25	In the presence of copper, increase atmospheric corrosion resistance
B	0.0005	Promotes bainite formation

The evolution of the chemical composition of microalloyed steels from 1959 to the present is shown in Table 2. Microalloyed steels present a large variety of complex combinations in their chemical composition (Nb-V, Nb-Mo, Nb-Cr) depending on the mechanical properties required.

The precipitation of carbides and nitrides occurs in three distinct stages during the microalloyed steels processing as is described in Table 3 [22,23]. These precipitates could be homogeneous, coherent, semi-coherent or incoherent with the crystalline lattice of steel. They can even precipitate in grain boundaries and dislocations, where they can later promote strain induced precipitation.

Modern studies have primarily focused on nanoprecipitates since they make a significant contribution to the yield strength [24]. The presence of precipitates (Ti, V, Nb) (C, N) inhibits the movement of the austenitic grain boundary and retards the grain growth at high temperatures [25]; this process impedes the movement of the dislocations and causes an increase in strength of the steel [26]. Other studies have determined that precipitates of TiN and Nb (C, N) have been effective

in inhibiting the growth of austenitic grain [11]. The austenite grain inhibition effect depends on the forming temperature of carbonitrides during the processing of steels.

The principal effects associated with the formation of Nb, V and Ti carbonitrides are listed in Table 4 and Figure 2 shows the solubility temperature of the most common precipitates in microalloyed steels. These effects depend strongly on the stability and solubility as a function of temperature processing. According to this figure, the VN, NbCN and TiC particles are stable at the typical normalizing temperature, around 900 °C, which induces a sufficient volume fraction of fine particles for grain growth controlling [27,28].

Table 2. Evolution of chemical compositions as a function of the API steel grade [21].

C	Mn	S	Si	Cu	Mo	Nb	V	Ti	Al	Cr	Ni	B	Grade
0.041–0.17	0.30–1.68	0.0002–0.03	0.02–1.39	0.02–0.31	0.005–0.14	0.018–0.06	0.042–0.21	0.002–0.01	-	0.02–0.157	0.005–0.8	-	X-65
0.037–0.125	1.44–1.76	0.001–0.015	0.14–0.44	0.006–0.27	0.01–0.3	0.051–0.092	0.001–0.095	0.009–0.03	-	0.007–0.266	0.02–0.23	-	X-70
0.028–0.142	1.52–1.90	0.001–0.009	0.17–0.31	0.015–0.20	0.05–0.3	0.038–0.090	0.002–0.1	0.007–0.024	-	0.015–0.12	0.02–0.75	-	X-80
0.025–0.1	1.56–2.0	0.001–0.0024	0.1–0.25	0.25–0.46	0.19–0.43	0.043–0.089	0.003–0.07	0.011–0.02	0.006–0.030	0.016–0.42	0.13–0.54	-	X-100
0.027–0.05	0.54–2.14	0.001–0.004	0.08–0.31	0.010–0.015	0.001–0.40	0.048–0.1	<0.025	<0.015	0.045–0.04	0.22–0.42	0.017–1.35	0.0013–0.0017	X-120

Table 3. Stages of carbides and nitrides precipitation during microalloyed steels processing [22,23].

Stage	Description
1	Formed during the liquid phase or after solidification process. Very stable precipitates, generally too coarse to influence on austenite recrystallization. Smallest can retard austenite coarsening during reheating.
2	Precipitation induced by strain during controlled rolling, retarding the austenite recrystallization and causing grain refinement.
3	Formed during or after austenite-ferrite transformation, nucleation in austenite-ferrite interphase or ferrite. Fine precipitation is observed.

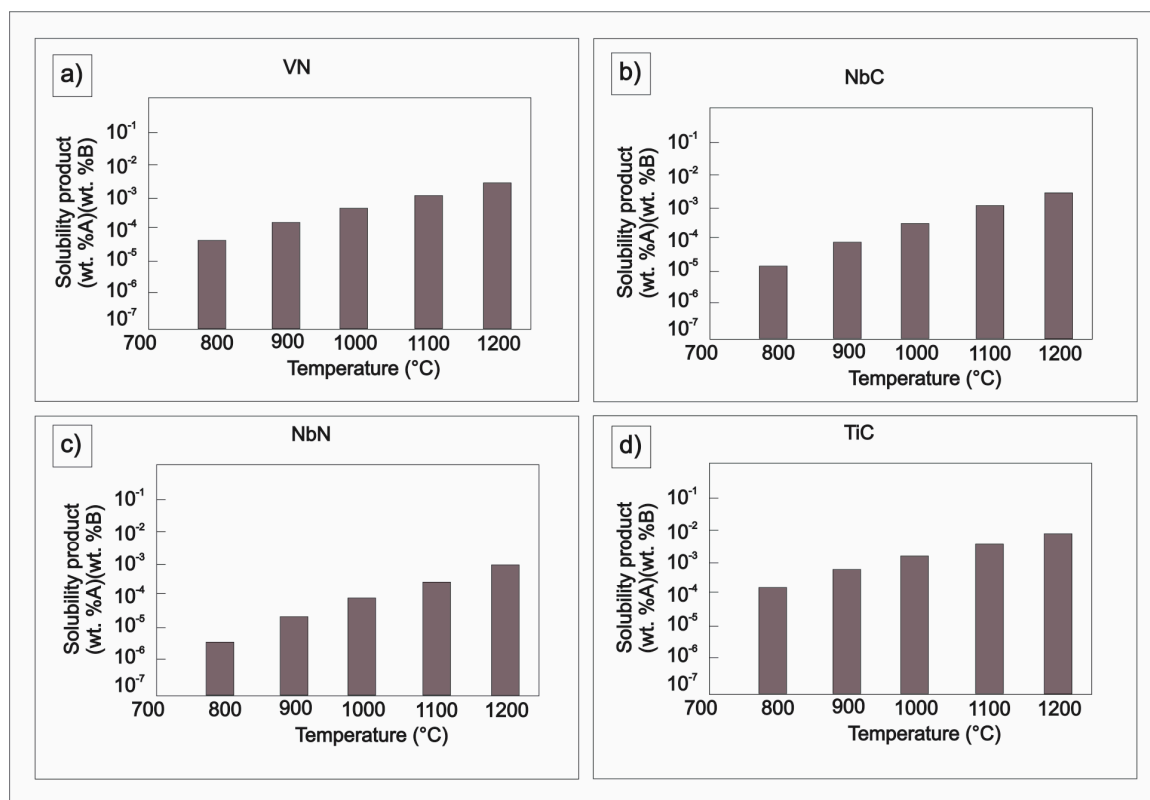


Figure 2. Carbonitrides solubility as a function of temperature, (a) vanadium nitride, (b) niobium carbide, (c) niobium nitride and (d) titanium carbide [27,28].

Table 4. The effect of carbides, nitrides and carbonitrides on steels processing [27,28].

Precipitate Type	Effect
Nb	Control austenite transformation during hot rolling processing
TiN	Pin and refine the grain size during high temperature austenitizing
VN, NbCN, TiC	Refines steels microstructure and grain size
Nb, NbCN	Increase recrystallization temperature during hot rolling
VC	Induces precipitation strengthening after normalizing
VN, VC, NbCN, TiC	Induce precipitation strengthening after hot rolling

Nb addition is used for grain refinement and precipitation strengthening, but this strengthening effect is reduced when Nb (C, N) precipitates during hot deformation. These precipitates retard the recovery and recrystallization of deformed austenite and increase the non-recrystallization temperature [29]. The principal role for Nb additions are: NbC and Nb (C, N) precipitation at austenite-ferrite transformation during cooling or cooling treatment that increases strengthening [30]; Nb solid solution and its carbonitrides precipitates retard the austenite grain growth and suppress austenite-ferrite transformation that cause a grain refinement.

On the other hand, small additions of Ti cause a finely dispersed nanoscale nitrides precipitation that restricts austenite grain growth at higher temperatures (1200 °C) [31]. Ti segregates during solidification of the steel and causes a local concentration inducing a precipitation of large TiN particles that cause a pinning effect and the formation of acicular ferrite producing a good heat affected zone (HAZ) toughness [32]. TiC precipitation can also cause strengthening; however, V is the most versatile precipitation strengthening element, and is effective in different compositions of microalloyed steels as well as in those with higher C content.

The Nb addition has a high influence on the transformation temperature of HSLA steels under normal processing conditions [21,33]. Nb in solid solution in austenite reduces the A_{r1} and A_{r3} transformation temperatures of C-Mn steel. This process causes a large austenite grain size that transforms in ferrite or bainite Widmanstätten. The presence of this microstructure conveys a lower fracture toughness than has been observed in Nb-treated steels finish rolled at temperatures around 1000 °C [34]. However, low temperature finish rolled steels containing a fine austenite grain size are able to use the Nb transformation effect in combination with that of bainite-forming elements such as Mo or B to form stronger and tougher steels. The use of controlled cooling reduces the amount of alloying elements required and the steels can reach strengths around 600 MPa [35].

In 2018, microalloyed steels with vanadium were studied, in which an increase in resistance up to 120 MPa was obtained. It was determined that the vanadium atoms in solution delay the bainite reaction at lower transformation temperatures (by 30–40 °C) within cooling rates of 1–50 °C/s [36].

3. Processing of Microalloyed Steels

One of the most efficient and commonly employed methods to improve and control the mechanical properties of steels is the TMCP. This technology has been developed and applied to the industry in a fast manner. A high production volume of steels has been manufactured through this process due to its excellent results. The main principles behind this process are the ability to refine the austenite grain size, increase the defect density, accelerate the precipitation of micro-alloying elements, and control the type of obtained phases [37]. This process has been used more and more, replacing the heat treatment techniques of normalizing, quenching and tempering the heat process. The TMCP helps to make cheaper and simpler the production process of low-carbon bainitic steels, in addition to providing high strength, high tenacity, and good weldability. One of the options to achieve these properties is to increase the microalloying contents, such as Nb, Ti or V; besides affecting austenite microstructural evolution, it contributes greatly to increasing precipitation hardening and dislocation density. One of the problems with high strength low alloy (HSLA) steels is the complex interaction between their hardening mechanisms, making it difficult to optimize parameters for their manufacture.

In order to maintain good control of the TMCP, a good understanding of the two processes involved is required; the complex interaction between strain precipitation of niobium carbonitride in austenite and static recovery [38–41] (Figure 3). The effect of initial austenite grain size and rolling temperature on the critical strain for recrystallization was studied by Tanaka et al. [42] and Kozasu et al. [43], and they reported excellent results in the year 1975, Figures 4 and 5.

Most microalloyed steels are manufactured by controlled rolling and accelerated cooling (TMCP). Severe low temperature rolling is often applied, which may negatively affect fracture toughness (ductile crack arrestability) and resistance to sour environments [44]. Consequently, other technologies have emerged such as the High Temperature Processed Steels [45].

Research by Kozasu et al. [43] showed that equivalent low temperature fracture toughness can be achieved at 1000 °C finishing temperature when 0.10 percent niobium is used compared with 800 °C finish rolling temperature (Figure 6).

In a TMCP, the mechanical properties are greatly affected by different parameters, such as rolling ratio, rolling temperature, cooling pattern, cooling rate and the coiling temperature. Among these factors, one of the most significant is the cooling temperature [46,47]. On the other hand, the temperature of the TMCP contributes to the precipitation of the microalloying elements [48–52].

In the year 2016, Misra and Jansto [53] reported a high strength low alloy (HSLA) steel. At a TMCP temperature of 579 °C, the reported yield strength (YS) was in the range of 701–728 MPa, tensile strength was 996–997 MPa, and elongation was 21–23% (Table 1) [54]. When the TMCP temperature was 621 °C, yield strength, tensile strength, and elongation were in the range of 749–821 MPa, 821–876 MPa, and 19–25%, respectively (Table 5) [54].

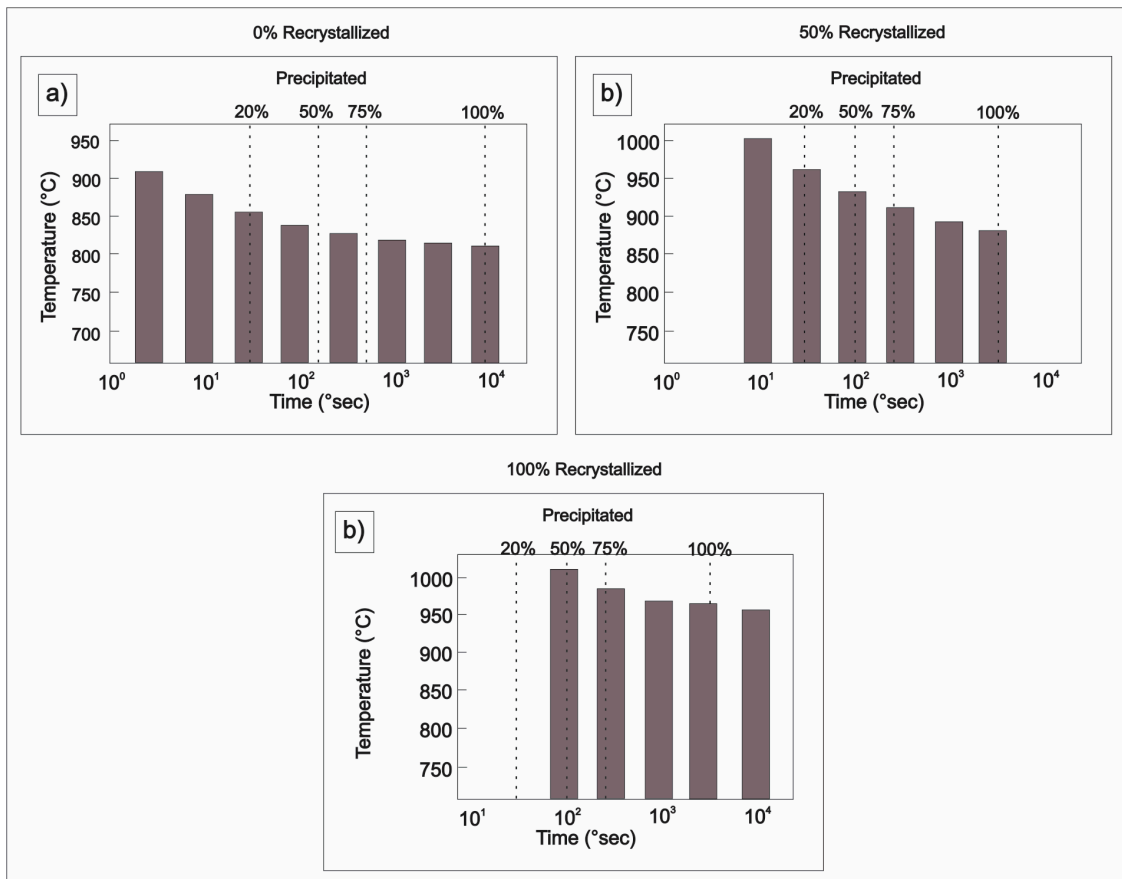


Figure 3. Isothermal recrystallization and precipitation in a columbium steel after 50% deformation. (a) 0%, (b) 50% and (c) 100%, recrystallized. The steel contained 0.10% C, 0.99% Mn, 0.040% Nb, and 0.008% N [38].

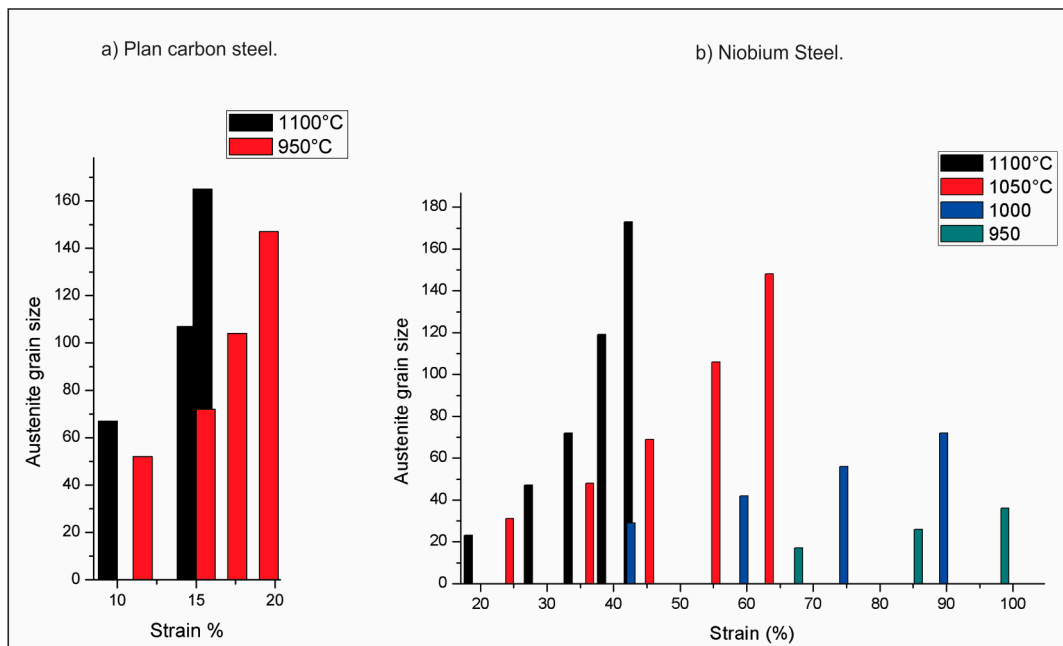


Figure 4. Effect of deformation temperature and initial grain size on critical amount of deformation required for completion of recrystallization in the (a) plain-carbon and (b) niobium steels [42].

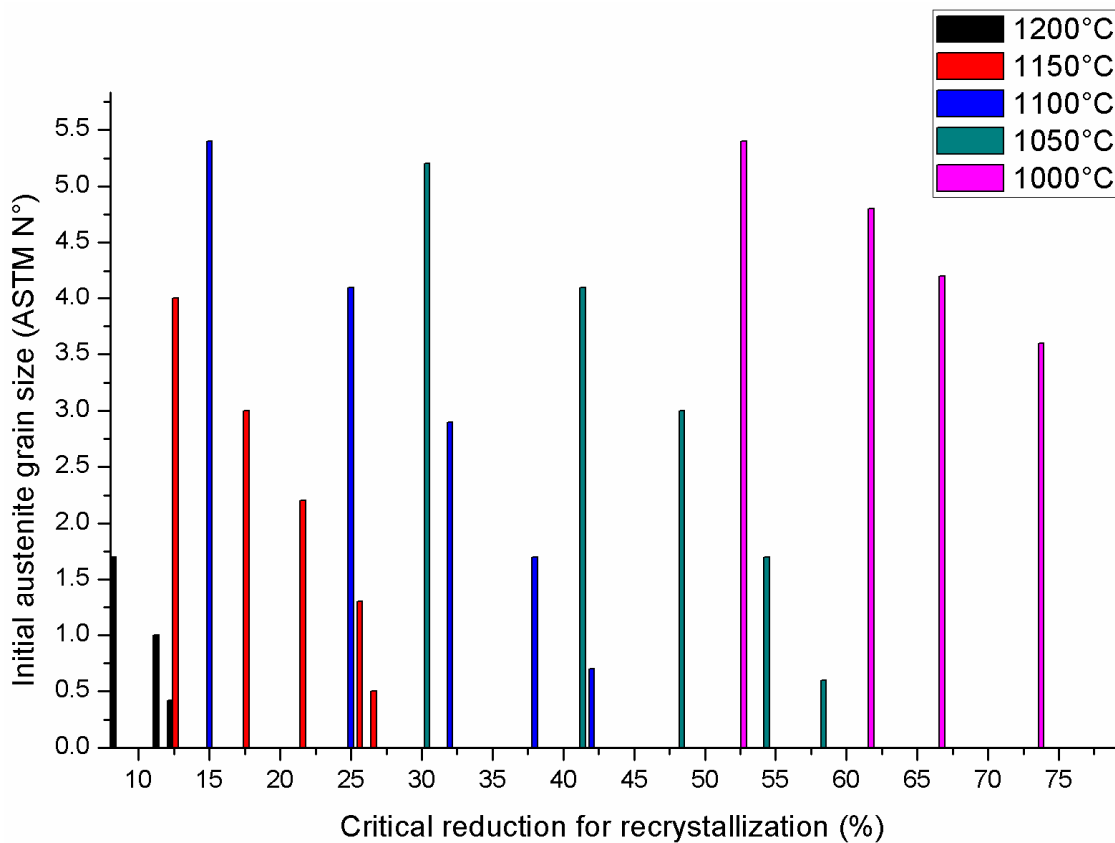


Figure 5. Effect of initial grain size on the critical rolling reduction needed for austenite recrystallization of a 0.03% columbium steel reheated to 1250 °C for 20 min. The initial grain size of the test plates was varied by rolling at higher temperatures [43].

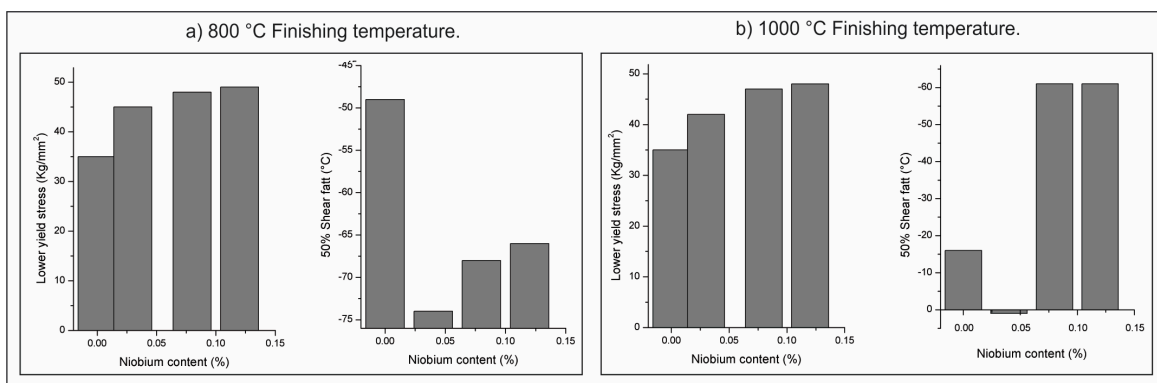


Figure 6. Effect of columbium on lower yield stress and transverse 50% shear fracture appearance transition temperature (FATT) for 20-mm thick steel with a 0.08% carbon, 0.25% silicon, and 1.50% manganese base composition. The reheating temperature was 1250 °C, (a) 800 °C finishing temperature, (b) 1000 °C finishing temperature [43].

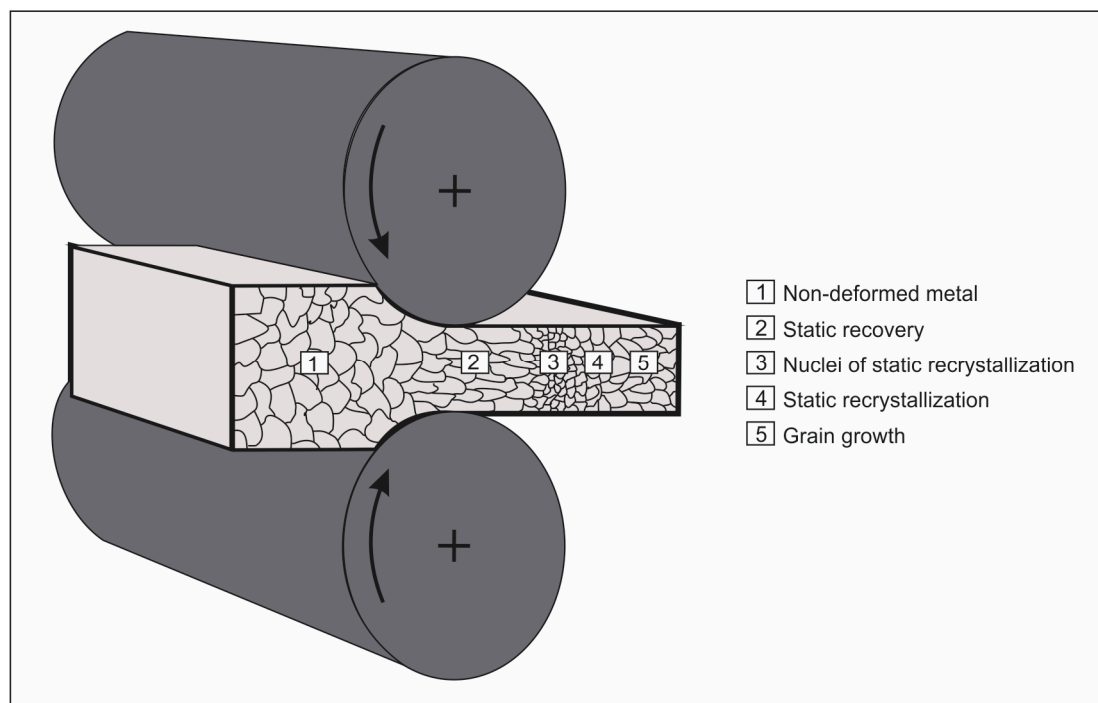
Table 5. Average yield strength, tensile strength, and elongation [54].

Temperature	579 °C	621 °C
Yield strength	701–728 MPa	749–821 MPa
Tensile strength	996–997 MPa	821–876 MPa
Elongation	21–23%	19–25%

Some works have focused on developing equations to determine the optimal parameters in specific compositions, such as Maubane et al. [55], who deduced an equation to calculate the instantaneous flow stress using multiple linear regressions. They observed that the main variables were dislocation density, precipitation hardening in ferrite [56], temperature, solid solution strengthening [57], and grain refinement through the lowering of the A_{r3} [58].

Some researchers [59] have reported that there are several ways to achieve excellent mechanical properties by designing materials incorporated with nanoscale microstructures. Three ways to obtain these properties are the use of finely distributed nanoparticles (based on precipitate strengthening), increase both the strength and ductility of the steels by designing an ultrafinely ferritic lamellae by the cold-rolling process and by altering the morphology, content and distribution, as well as concentration of the retained carbon in the austenite.

Grain size refinement in steels (Figure 7) holds a great deal of promise since it provides improved strength as well as toughness. Currently, ferrite grain refinement is achieved by a combination of controlled rolling and accelerated cooling. It has been found that this process can achieve a refinement of about 50% in steel plates of simple compositions. In the plate rolling process of a plain carbon-manganese (C-Mn) steel, grain size can be refined from 10 μm up to 5 μm when the plate is controlled rolled and accelerated cooled. This refinement in grain size increases the yield strength of the steel by about 80 MPa according to the well-known Hall–Petch relationship [60,61].

**Figure 7.** Schematic diagram of grain size refinement in steels.

A further fivefold reduction in grain size to about 1 μm is expected to increase the yield strength by another 260 MPa. Another fivefold decrease in grain size to submicron ranges would raise the strength by a further 586 MPa to levels >1000 MPa.

In view of the enormous advantages that are to be gained by the refinement of the grain size for simple steel compositions, researchers are active all over the world trying to produce ultrafine-grain ferritic steels. In Figure 8, a thermomechanical process is depicted with different strain levels and different cooling rates. It shows that deformation in the biphasic zone and air cooling produces a higher grain size in comparison with that the process with deformation above the Ar_3 transformation temperature and fast cooling.

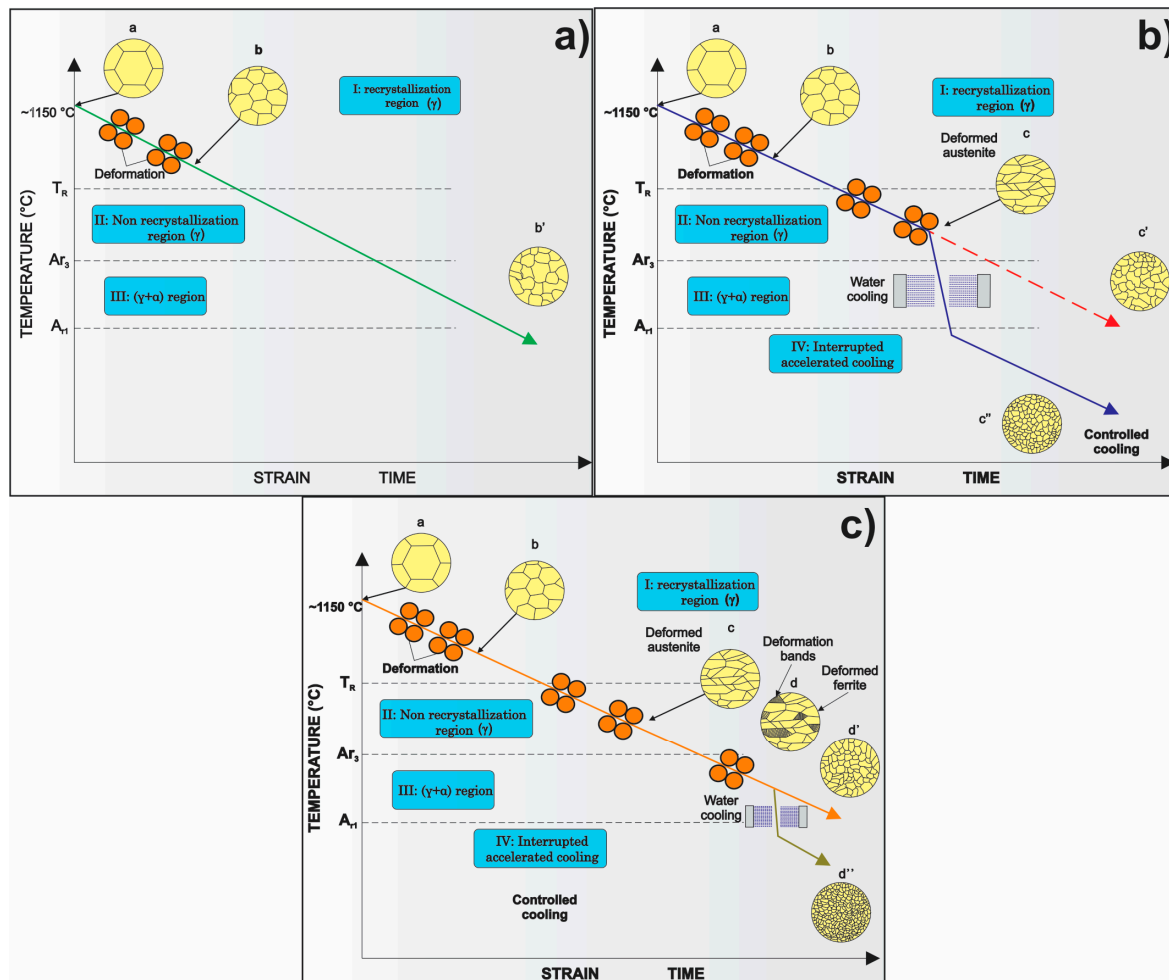


Figure 8. Grain size refinement as a function of rolling temperature and cooling rate. (a) Initial austenite grain size, (b) Austenite grain after rough rolling in recrystallization zone, (b') air cooled, (c) Deformed austenite grain just above T_R , (c') air cooled, (c'') water cooled, (d) Austenite grain after final rolling in non-recrystallization zone, (d') water cooled.

Presented below is a brief review of the current status of knowledge of this research field and the developments that have taken place in recent years regarding attempts to produce ultrafine grained ferritic steel. The following mechanisms have been proposed for obtaining ferrite grains as fine as $1\text{--}2\ \mu\text{m}$. These mechanisms are intended to operate during the thermomechanical processing of plain carbon steels and low carbon microalloyed steels.

Austenite is dynamically recrystallized, and the majority of deformation is obtained just above the austenite to ferrite transformation (Ar_3) temperature. This leads to the formation of ferrite grains that are $1\text{--}2\ \mu\text{m}$ in size.

High-strain-rate deformation is carried out just below the $\gamma \rightarrow \alpha$ transformation temperature. Due to the heat generated as a result of the high-strain-rate deformation, the ferrite transforms to

austenite for a while before transforming back to ferrite. This process, when carried out in a cyclic manner, leads to the formation of very fine ferrite grains.

The severe straining of ferrite is used to initiate dynamic recovery. However, this approach cannot lead to ultrafine grain sizes, but ferrite grain sizes of $\sim 3 \mu\text{m}$ can be achieved. This occurs because further grain refinement in ferrite is very difficult due to the low strain-hardening exponent and the higher stacking fault energy of ferrite.

The deformation of coarse-grained austenite beyond a critical strain leads to the intragranular nucleation of ferrite inside the austenite grains, leading to considerable refinement of the ferrite grains. This mechanism is believed to operate while producing a layer of ultrafine ferrite at the surface of a thin strip. This refinement procedure requires austenitization at high temperatures to produce coarse austenite grains. The strip is then cooled to very near the A_{r3} temperature of the steel and is rolled at that temperature. An extremely high nucleation density of ferrite on the dislocation substructure within the coarse austenite grains is obtained due to the intense localization of shear strain in the layers close to the surface. This processing sequence results in a layer of ferrite approximately $1 \mu\text{m}$ in diameter close to the surface, while the core of the strip transforms to a more normal microstructure of coarser ferrite or bainite, depending on the cooling rate and composition of the steel.

The unique features of this method of production of ultrafine-grained steel is that it employs characteristics that are not generally considered to be desirable in the conventional controlled rolling of steel, namely, a large austenite grain size, supercooling of the austenite, and high friction at the work-piece/roll interface.

Water quenching of the surface layer of the steel before the penultimate hot-rolling pass is another way to transform the surface layer of a strip into very fine ferrite grains. Heat from the core of the plate raises the surface temperature, so that the ferrite recrystallizes during the final pass, leading to a grain size of about $2 \mu\text{m}$. This mechanism of refining the grain size at the surface is used when producing HiArrest plates (Nippon Steel, Kawasaki, Japan), which possess superior crack-arresting properties.

An altogether different route of obtaining ultrafine grains is the cold rolling and warm annealing of a martensitic structure. However, the limitation of this processing route is the achievement of the martensitic structure in plain C-Mn steel, which limits the thickness of the sheet.

In recent studies, a 0.013% Nb, C-Mn steel was thermomechanically processed in an attempt to obtain very fine grains of ferrite. The resulting microstructure was characterized.

The effect of Nb content on the austenite microstructural evolution during hot deformation has been studied in the past [62], having two different percentages of Nb (0.04 and 0.11%); it is observed that this difference does not affect the grain size; however, their mechanical properties are greatly affected. A difference in the cooling temperature leads to a large difference in the obtained mechanical strength. They observed that, for the alloy with low Nb content at $700 \text{ }^\circ\text{C}$, the lowest strength values were obtained, while at a temperature of $600 \text{ }^\circ\text{C}$ they observed an increase of 90 MPa in the YS and finally for a temperature of $500 \text{ }^\circ\text{C}$ the YS decreased 20 MPa. For the alloy with high Nb content, the tendency was similar, although the increase in strength was greater, raising 140 MPa as the temperature descended from 700 to $600 \text{ }^\circ\text{C}$. This corroborates the great impact that the microalloying elements provide for improving the strength of HSLA steels.

Due to the needs of the industry to manufacture stronger and thinner steels, a new technology called ultra-fast cooling (UFC) has been developed in the last few years to obtain steels with better mechanical properties. In 2004, CRM Group implemented a UFC technology to improve control and efficiency in the manufacturing of high strength steels [63]. By increasing the cooling rate, they were able to produce cheaper high strength steels (up to 850 MPa); this was done with cooling rates of around $300 \text{ }^\circ\text{C/s}$. Likewise, Mohapatra et al. [64], applied UFC technology to a hot stationary AISI-304 steel plate by using air atomized spray at different air and water flow rates. They observed that the water flow rate or spray impingement density are found to be an important parameter during high temperature air atomized spray cooling. Other authors [65] have focused their research to find an analytical method, in function of the droplet diameter from a fundamental heat transfer perspective based on the premise

that a spray can be considered as a multi-droplet array of liquid at low spray flux density, for a spray evaporative cooling as an alternative to conventional laminar jet impingement cooling.

Techniques such as physical simulation have been broadly employed to optimize parameters such as casting, reheating, rolling, and accelerated cooling conditions. Physical simulation has proven to be a powerful tool in the design and manufacture of new linepipe steels by reducing production costs and improving performance [66].

4. Development of Steels throughout History

Through history, great developments have been made concerning the manufacture processes of microalloyed steels, which have brought great benefits to the development of society, owing to their high strength provided by the alloying elements in their composition. Figures 9 and 10 show a brief summary of the most relevant events spanning from the year 1865, with the first patent of a steel alloy with Chromium (Cr), through the formation of the group for the exchange of information called steel treaters club, which later became the American Society for Metals (ASM), until the decade of the 1970s.

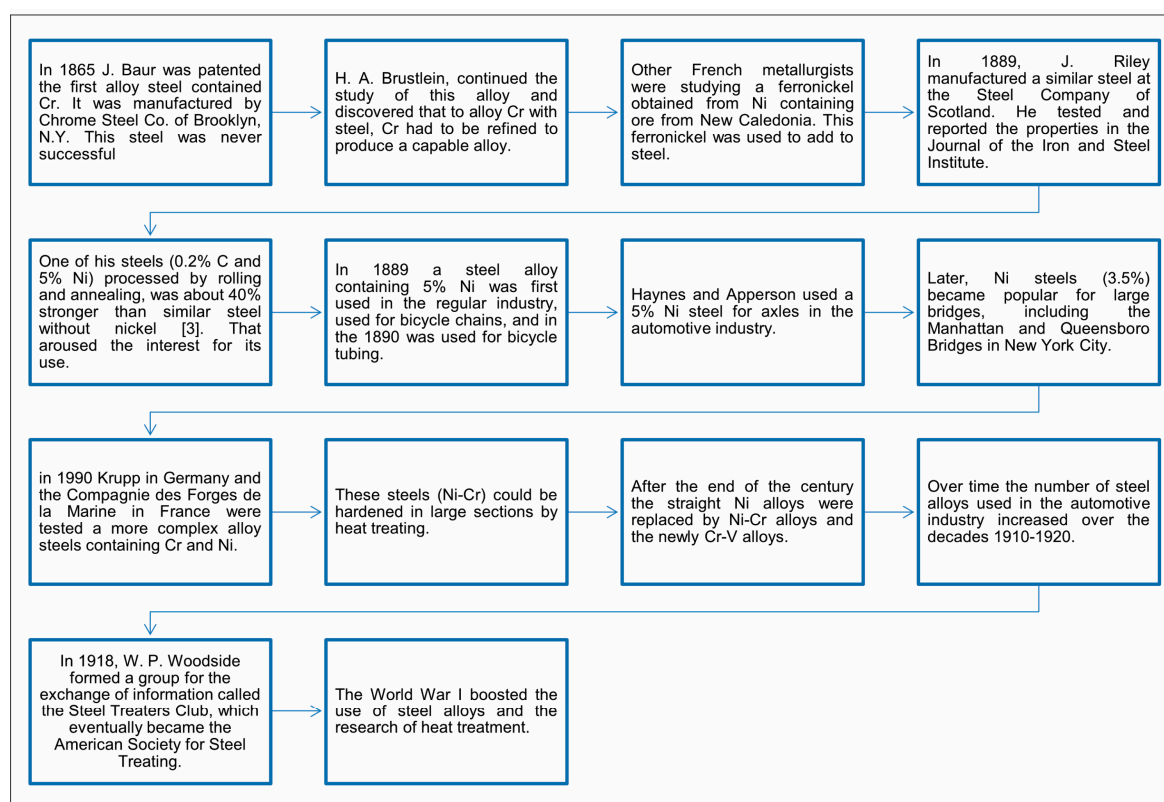


Figure 9. Brief history from 1889 to 1918.

Research in the field of microalloyed steels has increased over the decades, focusing on improving their strength and environmental resistance by precipitates and microstructure controlling. Table 6 presents an analysis of some relevant topics reported in the reviewed literature, ranging from the decade of the 1940s to the present, making a strong emphasis on the development of microalloying elements, control of microstructure, thermal and thermomechanical treatments, as well as the influence they have on steel properties.

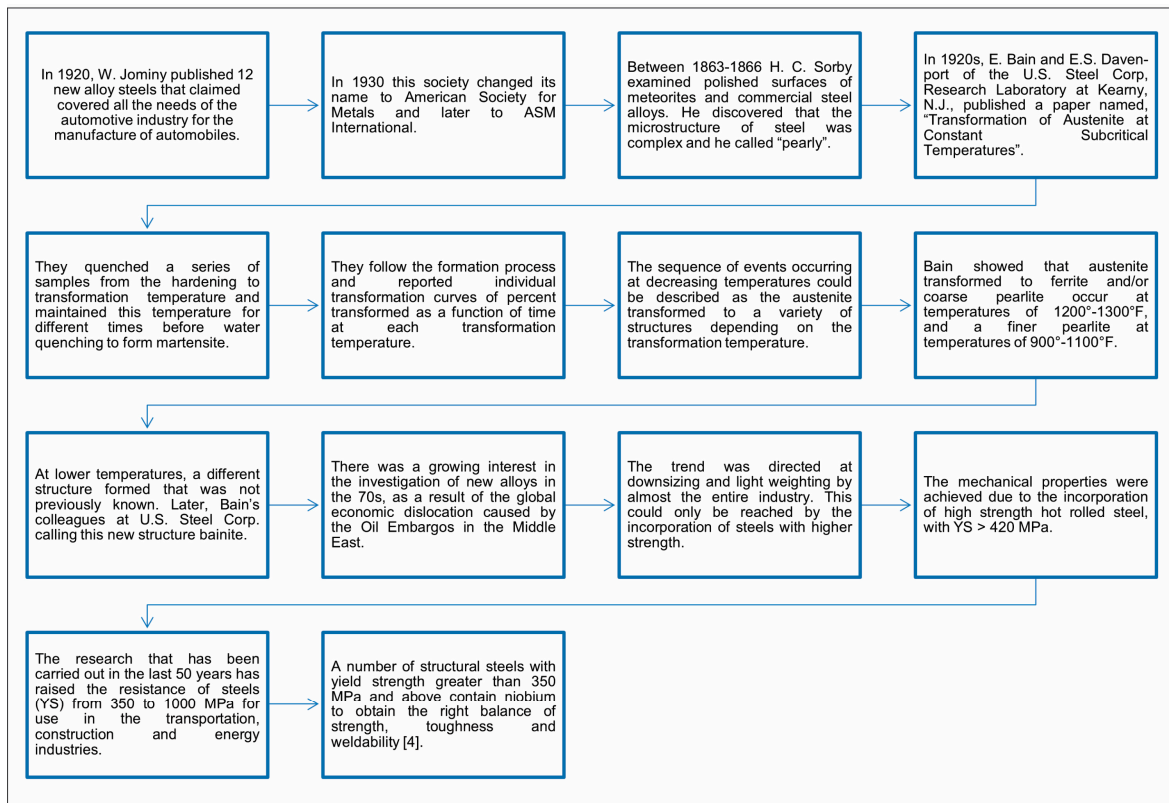


Figure 10. Brief history from 1920 to the 1970s.

Figure 11 shows the development of HSLA steels from 1940 to 2000, the data of which were published and included in the proceedings of international conferences [67–71].

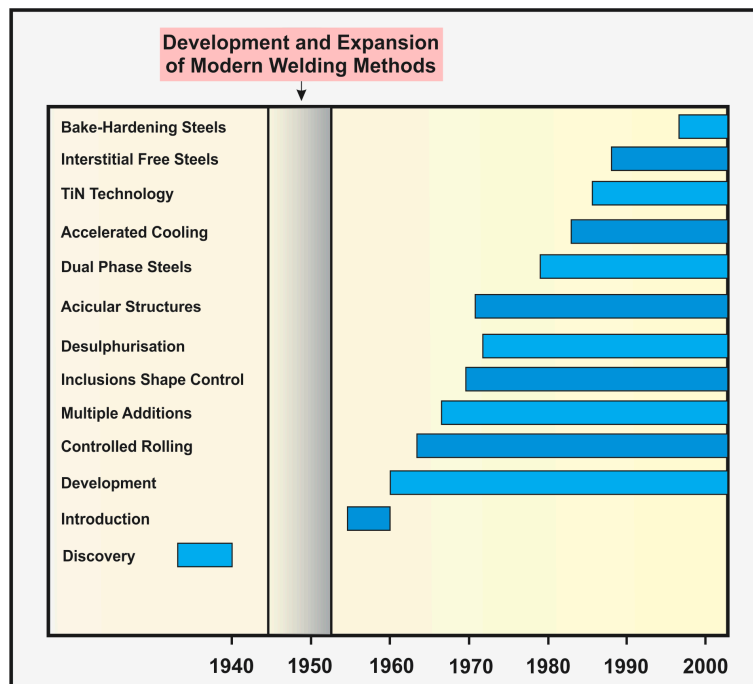


Figure 11. Development of the HSLA steels from 1940 to 2000 published in the proceedings of international conferences [67–71].

Table 6. Relevant topics reported in literature from the 1940s to the present [1–167].

Decade	Relevant Topics
1940s	Patent No. 2,264,355, “Steel” by F.M. Becket and F. Russell.
1950s	Deformation and ageing of mild steel. Cleavage strength. Metallurgy of Microalloyed steel. Columbium(Nb)-treated steels. Effect of small Nb additions to steels.
1960s	Small Nb addition to C-Mg steels. Dislocations and plastic flow. Effects of controlled rolling. Strong Tough Structural Steel.
1970s	Theory of hydrogen embrittlement. New model for hydrogen embrittlement. Assessment of precipitation kinetics. Stages of the controlled-rolling. Control of inclusions. Controlling inclusions by injecting Ca. Materials for hydrogen pipelines. Analysis of hydrogen trapping.
1980s	Recrystallization of austenite during hot deformation. Hydrogen degradation. Effect of accelerated cooling. Niobium carbonitride precipitation. Environmentally assisted cracking.
1990s	Specifications requirements for modern linepipe. Strain induced precipitation of Nb in austenite. Hydrogen interactions with defect. Nitrogen in steels. TiN-MnS Addition for Improvement toughness. Sulfide Stress Cracking. Softening and flow stress behavior. Influence of titanium and carbon contents. Titanium technology.
2000s	Effects of coiling temperature on microstructure. Effects of sulfide-forming elements. Effect of chromium on the microstructure. Hydrogen induced blister cracking. Effects of thermo-mechanical control process. Influence of Ti on the hot ductility. Trap-governed hydrogen diffusivity. Comparison of acicular ferrite and ultrafine ferrite. Influence of Mo content. Ultra-Fast Cooling. Role of Nb, B and Mo hardenability. Ductile crack propagation in pipes. Effect of bainite/martensite mixed microstructure. Effect of tempering and carbide free bainite. Microstructural evolution. Influence of Mn content. Steels processed through CSP thin-slab technology. Effect of Mo on continuous cooling bainite transformation. Correlation of microstructure and Charpy impact properties. Dual phase versus TRIP strip steels. The effect of niobium in Castrip [®] steel. Spray evaporative cooling.

Table 6. Cont.

Decade	Relevant Topics
2010s	Ti-alloyed high strength microalloyed steel. Hot strip steels. The first direct observation of hydrogen trapping sites. Evolution during thermomechanical processing. Ultra-High Strength X120 pipeline steel. Niobium high carbon applications. Modern HSLA steels. Ultra-low Carbon steels. Ultra-Fast Cooling. Mechanical anisotropy in steels. Effect of dissolution and precipitation of Nb. Influence of nanoparticle reinforcements. Reversible hydrogen trapping. Strengthening by multiply nanoscale microstructures. Effects of TMCP schedule on precipitation.

5. Sulfur Content in Microalloyed Steels

Some applications of microalloyed steels, such as X-80 or ultra-high strength X-100/120, require very high Charpy V-notch or DWTT (Drop Weight Tear Test) energies for ductile fracture control and can only be achieved in clean low sulfur steels [72]. Currently, this technology has advanced enough to obtain very low levels of sulfur (less than 10 ppm), allowing the industry to produce large quantities of steel with high strength and excellent toughness.

Over the years, the sulfur content has been reduced in the alloys of microalloyed steels, which has allowed for continuously improving the toughness of steels (Figure 12).

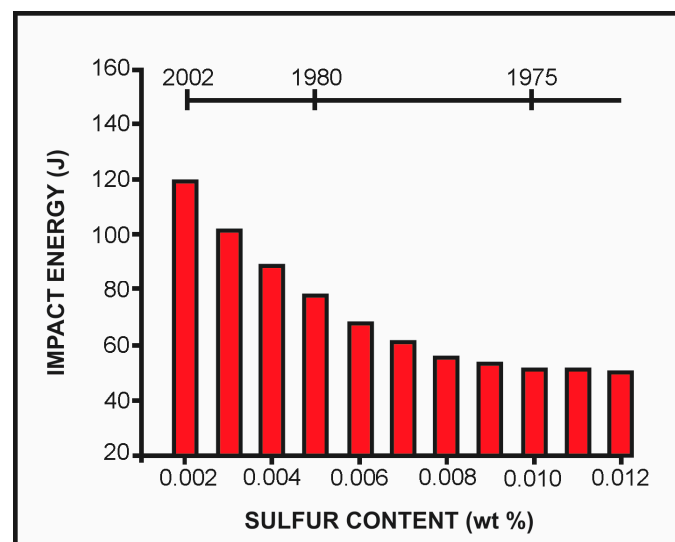


Figure 12. Effect of sulfur content on toughness of linepipe through the years.

Advances in desulfurization have been of great importance because they contribute to the control of the microstructure. The control by sulfides has been considered to improve the toughness of microalloyed steels [73,74], microstructure of heat-affected zone of welded metals [75], silicon steel sheets [76], etc.; this is mainly due to the fact that sulfur can retard the growth of the austenitic grain since it is relatively stable between the precipitates at high temperatures of rolling, besides promoting the formation of intergranular ferrite.

Some researchers have continued to investigate the effects of sulfur content on microalloyed steels. Tsunekage and Tsubakino [77] reported nine ferrite-pearlitic microalloyed steels, in which the sulfur contents were varied from 0.001 to 0.176 mass %, compensating for the increase in the formation of MnS inclusions with manganese in the amount equivalent to atomic % of S content. They determined that the Charpy impact values in the longitudinal direction of the studied steel increased with the addition of sulfur between 0.05–0.1 mass %; however, in the transverse direction, the Charpy impact values were reduced with content of 0.1 mass % of sulfur. On the other hand, the Charpy impact values in the transverse direction of the steel with 0.1 mass % sulfur content increased with the addition of Ca or Mg without affecting the Charpy impact values in the longitudinal direction.

Tomita et al. [75] also performed studies on the influence of MnS precipitates coupled with TiN precipitates on steel for offshore structures and thus clarify which are the main mechanisms responsible for the improvement of the heat affected zone toughness. This study determined that the heat affected zone contained intragranular ferrite formed by TiN-MgS and intergranular ferrite inhibited by ultra-low niobium. These conditions reduced the size of the fracture facet of the heat affected area and improved the steel toughness.

6. Mechanical Properties of Microalloyed Steels

The main purpose for designing microalloyed steels was to develop a good combination of mechanical properties (high strength and good toughness) in the as rolled condition, which allows for reducing the amount of required material, reduces the weight in specific applications, fabricates more effective mechanical designs, and reduces costs. These types of steels can achieve the same strength as cold worked C-steels and produce similar mechanical properties to quenched and tempered air cooled hot worked steels.

In the 1960s, the publications of Hall [60], Petch [61] and Cottrell [78] provided the first real understanding of the variables that control the mechanical properties of crystalline materials. The Hall–Petch equation allows for determining the yield strength as a function of the ferrite grain size d :

$$\sigma_y = \sigma_0 + k_y d^{-1/2}$$

where σ_0 and k_y are experimental constants. An example of the grain size effect on the strength of a plain carbon steel and C-Mn-Nb steel is shown in Figure 13.

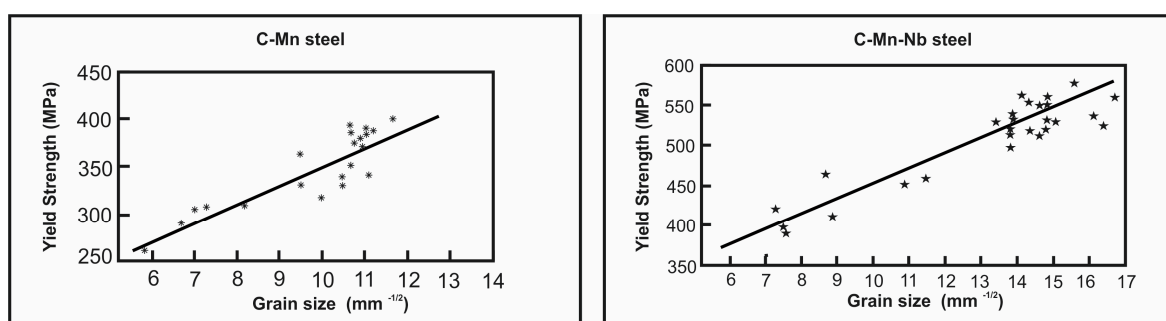


Figure 13. Experimental Hall–Petch relationship of grain size effect on strength of plain carbon and microalloyed steels [79].

The austenite grain size is critical to obtain a specific final microstructure, strength level and toughness of microalloyed steels after being thermomechanically processed and controlled cooling.

The earlier microalloyed steels avoided transformations of acicular microstructures, in the years 1960–1980, microstructures of microalloyed steels were ferrite-pearlite principally, obtained after hot rolling and air cooled [80]; this was triggered due to the low hardenability, reaching yield strength up to 450 MPa, and the principal characteristic was higher C content and relatively high

Mn levels [17]. The principal applications were for pipeline and automotive components, but the constant requirements of high mechanical properties demanded a higher strength microstructure such as non-polygonal ferrite, acicular ferrite, bainites and martensites achieved by higher hardenability and high cooling rates, using water cooling as principal media. The common processes for improving mechanical properties were interrupted accelerated cooling and interrupted direct quenching, controlling the cooling rate independently of microstructural control and composition. With the evolution of controlled rolling and high cooling rate, a low C steel containing 2 wt % of Mn could reach 690 MPa without heat treatments [81].

The first report on the use of microalloyed steels was a normalized API Grade X-52 vanadium steel around 1952 and extended later to X-56 and X-60 API Grade [82].

In the last two decades, high strength steels thermomechanically processed and accelerated cooled were developed with yield strengths in the range of 350–800 MPa and substituted the mild steels with lower yield strength (150–200 MPa) [83] for their use in the transportation, construction and energy industries. Figure 14 shows the evolution of the mechanical properties of pipeline steels.

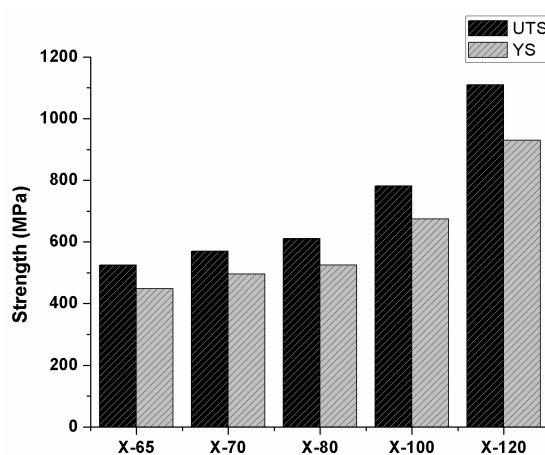


Figure 14. Mechanical properties of pipeline steels [19].

In order to achieve higher mechanical properties, the transformation temperatures should be lowered by addition of microalloying elements as well as fast cooling quenching to promote the formation of martensite–bainite. The addition of V had a small effect on transformations temperature due to the formation of nitrides in higher N content [84]. The evolution of common microstructures used for pipeline steels and its processing is shown in Figure 15 as a function of API grade steels.

Controlled rolling processes have been developed and used in the manufacture of microalloyed steels, with the basic objective of refining and/or deforming the austenite grains during rolling to obtain fine grains of ferrite during cooling.

The mechanical properties, as well as the fine-grained microstructure, can be modified by the strict control of TMCP (heating temperatures, percentage of reduction, time between rolling passes, start and end of rolling) and accelerated cooling (cooling start temperature, cooling rate, final cooling temperature) [85,86]. Depending on these conditions, different microstructural combinations can be obtained [50,87].

In order to optimize the control of TMCP, a clear understanding of the behavior of austenite recrystallization, precipitation kinetics of microalloying elements and the effect of cooling rate on the final microstructure of these steels is necessary [88]. Some studies have reported that deformation in the non-recrystallization region may increase the number of dislocations and induce precipitation during the rolling process [89–91]; this also increases the fraction of acicular ferrite volume after cooling. Figure 16 shows a processing comparison of steels obtained via conventional rolling, controlled rolling and controlled rolling-accelerated controlled cooling (CR-ACC). The main benefits of the CR-ACC

process come from the band deformation that occurs in the austenite deformed grain that acts as a nucleus for ferrite grains during accelerated cooling and consequently facilitates the formation of finer ferrite grains.

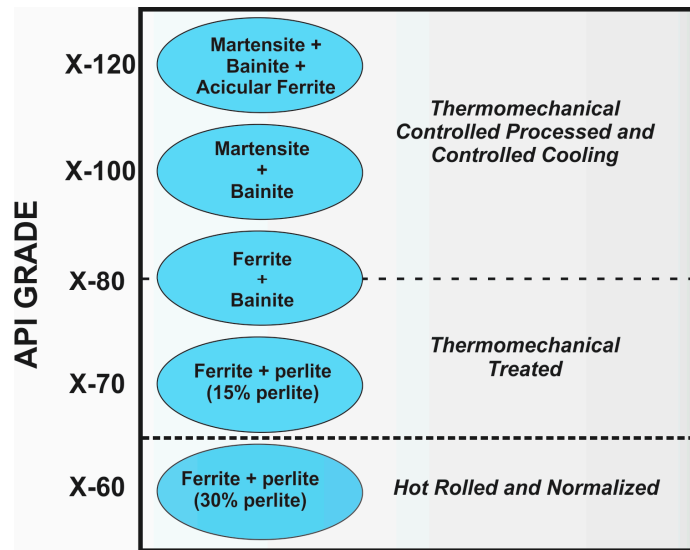


Figure 15. API grade steel evolution as a function of microstructure and thermomechanical processing.

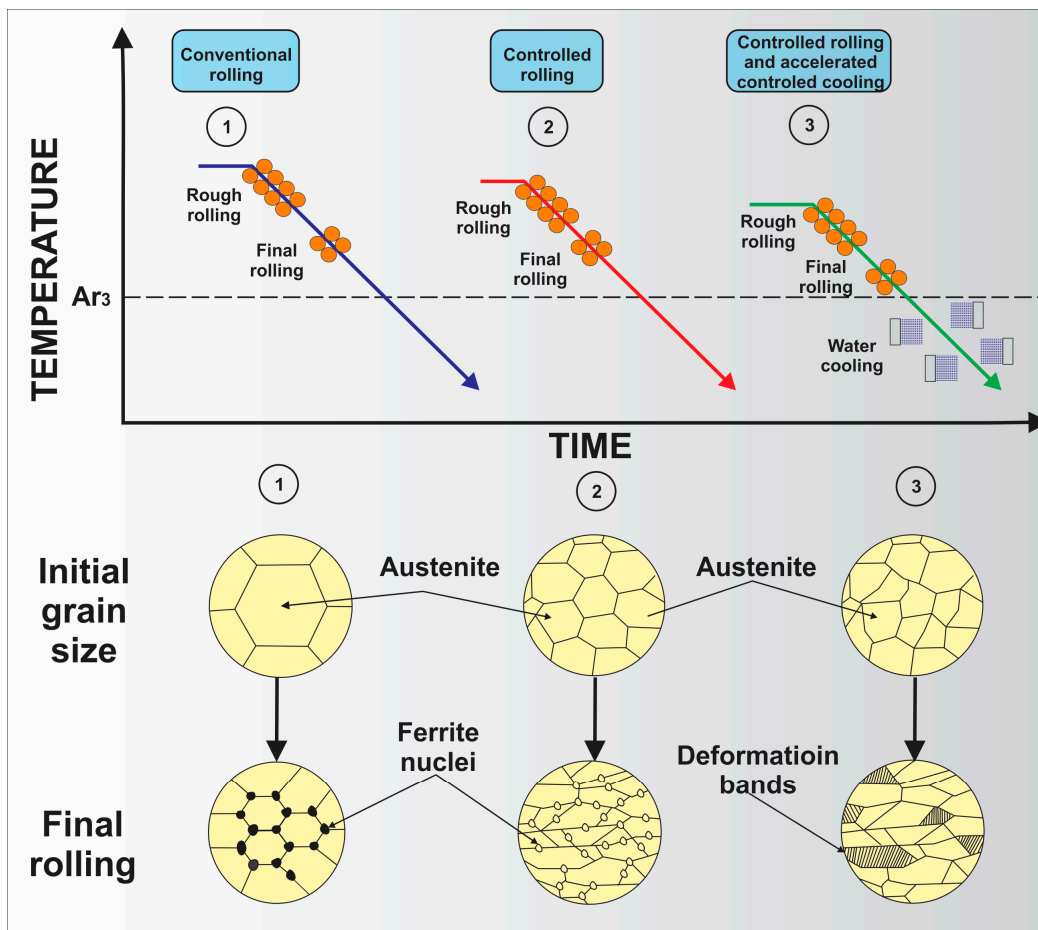


Figure 16. Thermomechanical controlled processing.

In the same way, the total degree of deformation has a great influence on the strength and toughness, Manuel Gomez et al. [92] studied the effect of hardening of the austenite in an API 5L-X80 microalloyed steel, during and at the end of the thermomechanical processing, as well as in the final microstructure after cooling. They observed that the ferrite grains are finer and more equiaxed when the austenite is severely deformed during the final rolling (below T_{nr}); however, when the deformation percent is lower, a large number of acicular structures are generated due to precipitation of (Ti, Nb) (C, N) with particles sizes around 4–6 nm, improving the balance between the mechanical properties, reaching yield strengths even up to 840 MPa. Many authors have observed that the high density of dislocations in austenite displaces the transformation of the products of bainitic microstructures to acicular ferrite [93,94], or even polygonal ferrite and pearlite [95].

Figure 17 illustrates an experimental TMCP for a high strength microalloyed steels. Figure 17 ①, shows an austenitizing process at 1200 °C for break down the dendritic microstructure obtained from melting slab and air cooled. Figure 17 ② represents a normalized treatment at 1200 °C for 1 h and rough rolling above the recrystallization temperature and final rolling in the non-recrystallization temperature and air cooled. After this process, a quenching treatment was carried out from 900 °C using as cooling media oil-water emulsion and water (Figure 17 ③). The microstructures obtained were formed mainly by bainite–martensite and acicular ferrite reaching a UTS (Ultimate Tensile Strength) around 1100 MPa.

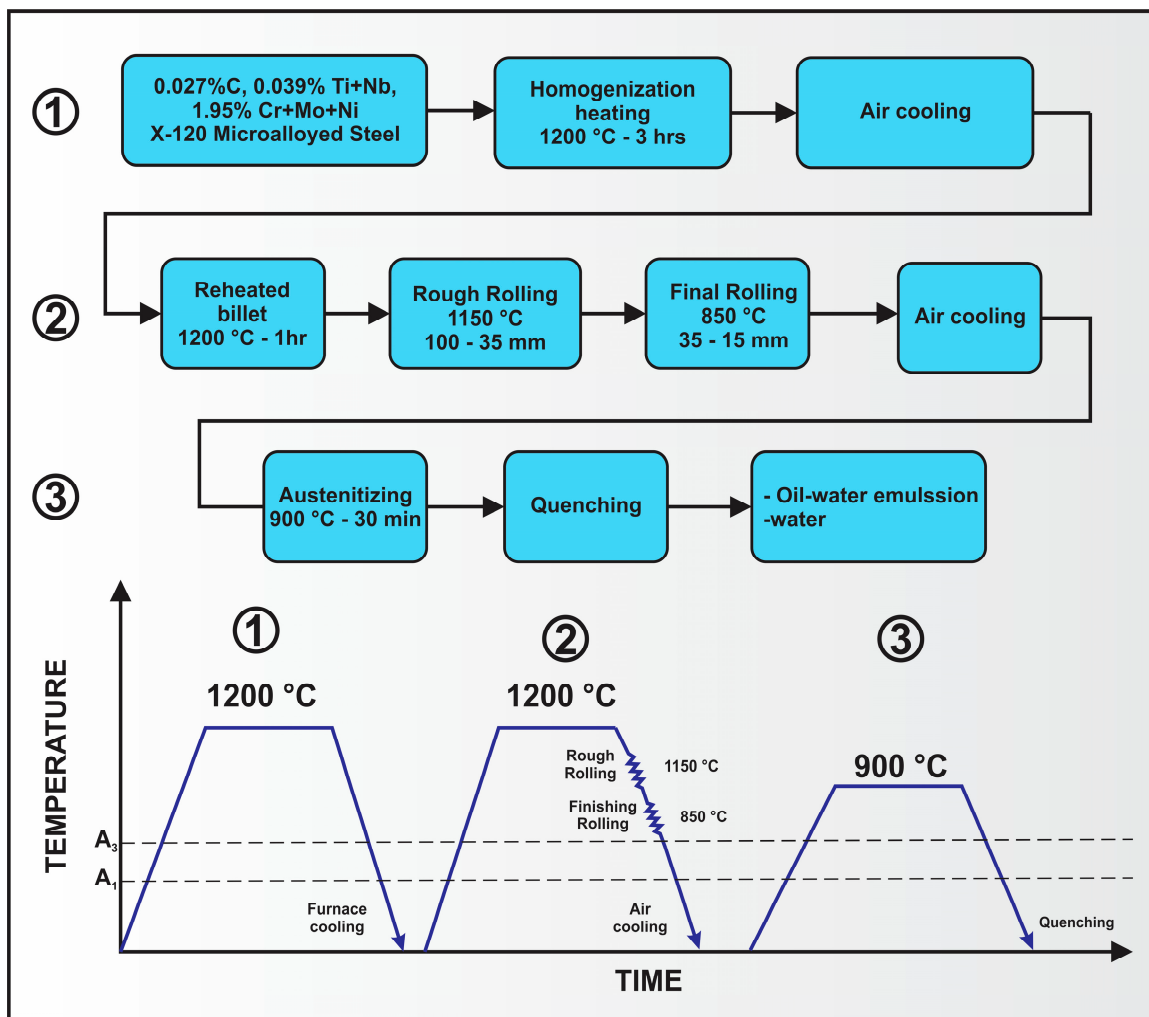


Figure 17. ① Schematic of steel processing, ② heat billing and air cooling, ③ thermomechanical processing and quenching processes.

In the following pictures, micrographs obtained by different API grade steel with different processing and cooling rates [96] of unpublished work are compared. Figure 18a shows an API X60 grade steel with a UTS around 425 MPa and a ferrite-pearlite microstructure; this steel was hot rolled and cooled in air. The use of thermomechanical processing allowed for achieving higher API grade steels; as it is shown in Figure 18b,c, those steels were thermomechanically controlled processed and cooled in oil and in an emulsion of water-oil, reaching a strength around 600–700 MPa and microstructures formed mainly by bainite–martensite. Figure 18d show the microstructure of API X120 steels. It consists of a complex mixture of bainite–martensite and acicular ferrite, allowing it to obtain a good combination of strength, ductility and toughness. This steel was thermomechanically controlled processed and cooled in water, obtaining strength values over 1100 MPa and an absorbed impact energy of 84 J.

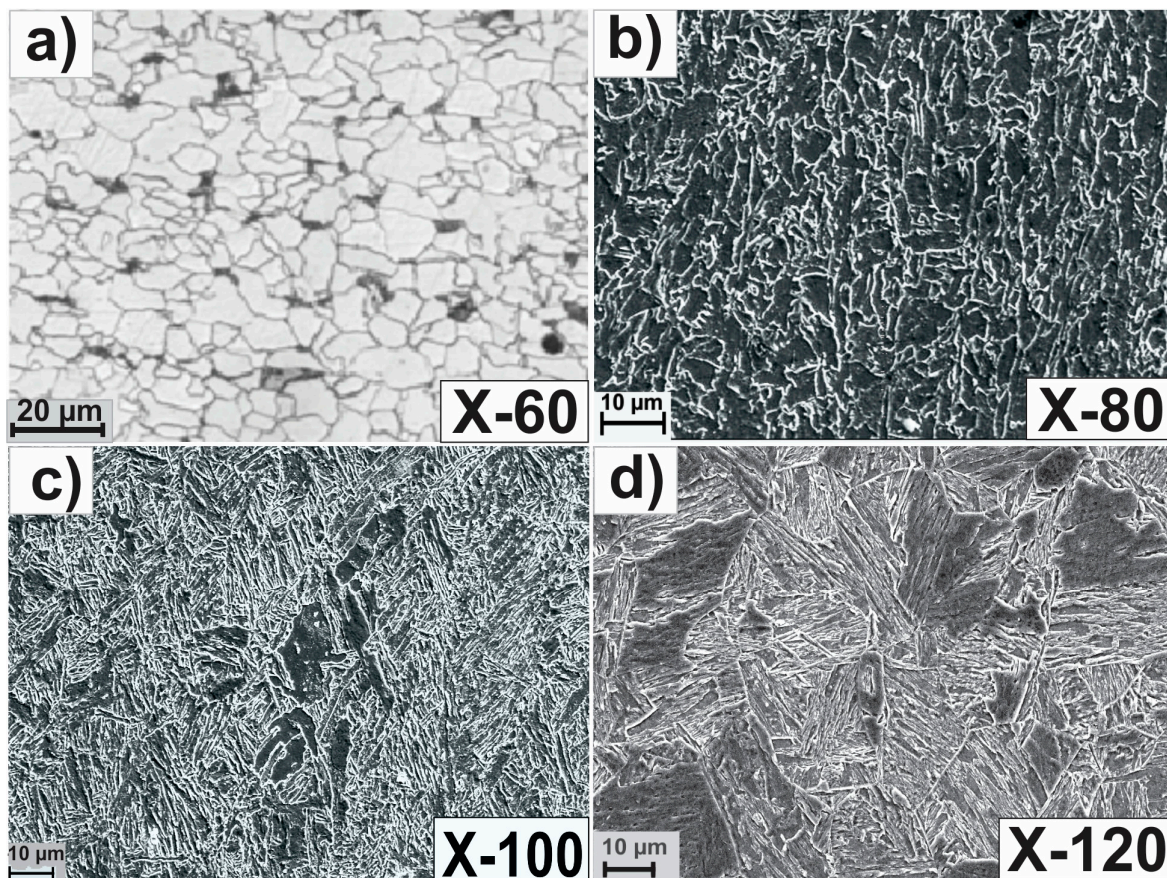


Figure 18. A typical microstructure of API microalloyed steels as a function of thermomechanical processing. (a) ferrite-pearlite, (b) ferrite-bainite, (c) acicular ferrite-martensite, (d) acicular ferrite-bainite-martensite.

The addition of microalloying elements may intensify the effects generated by the TMCP due to the displacement of the transformation temperatures (A_1 – A_3), and as a result the austenite transformation to acicular ferrite occurs at lower temperatures during the cooling. This process can generate a transformation of finer ferrite grain. A lower transformation temperature induces the formation of non-polygonal ferrite, acicular ferrite, bainite and martensite. However, to generate this type of microstructure, high hardenability and high cooling rates are required [17].

In addition to the ferritic grain refinement, the micro-alloying elements promote precipitation hardening and solid solution strengthening [97]. This precipitation hardening effect can be increased by the addition of Ti and Mo, due to the Nano-precipitation of (Ti, Mo) C according to Kim [89],

which are thermally more stable compared to other types of carbonitrides, because they are more homogeneous and thinner. However, increasing Ti, Mo and C content conveys a decrease of impact toughness properties due to the improvement in strength of the steel.

It has been observed that the C content decreases toughness due to the high-volume fraction of martensitic-austenitic microconstituents [98,99]. In order to compensate the decrease in toughness, it is necessary to increase Ni and Cr content. Previous studies have shown that Cr promotes a higher toughness and could increase the amount of acicular ferrite. On the other hand, the addition of Mn and Ni can reduce the transition temperatures, therefore obtaining good toughness values at low temperatures [100]. According to other studies [101,102], the energy absorbed in the impact tests is also affected by the type, volume fraction, size and morphology of the individual phases that composed the material. Kang et al. [103] observed that materials with finer ferrite grain sizes provide greater absorbed impact energy.

The addition of Nb and Mo is used to achieve a favorable combination of strength and toughness. It is well known that Nb in microalloyed steels improves microstructure and precipitation hardening as well as grain refinement. Chen et al. [33] studied the effect of Nb on the formation of ferrite-bainite in a low-C HSLA steel and concluded that Nb (C, N) precipitates retard the formation of ferrite-bainite during accelerated cooling processes. Wang et al. [104] studied the influence of Nb on the microstructure and mechanical properties of low-C steels with bainitic and air-cooled microstructure and concluded that the amount of bainite is increased by the addition of Nb, and the agglomeration of precipitates of Nb are finer in this type of steel.

On the other hand, the addition of Mo reduces the initial temperature of bainitic transformation [105]. The addition of Mo in steels can separate the bainitic transformation lines and bainitic microstructures can be obtained over a wide range of cooling rates, and in combination with Nb improve their hardenability [106,107].

Ti is an effective and economical microalloying element, due to the fact that it has a great influence on the microstructural evolution during the manufacturing processes that change the final mechanical properties [103]. Ti as well as B is deliberately added to improve the hot ductility of microalloyed steels and Nb usually is added to prevent cracking on the surface during continuous casting. It also usually induces precipitation at high temperatures in austenite phase [108]. Along with the addition of Nb and Mo, microalloyed steels could reach yield strengths above 700 MPa due to the coprecipitation of TiC.

The accelerated cooling modifies the transformation microstructure [109,110], obtaining microstructures of acicular ferrite and dual phase, with martensitic-bainitic microconstituents dispersed in a polygonal ferrite matrix. Li [111] has studied the impact of TMCP on microalloyed steels, and, with the addition of Nb and Ti, they obtained a wide range of mechanical properties through microstructural changes, depending on the cooling rate. Compared to continuous cooling, interrupted cooling was the most suitable for the generation of dual microstructures (polygonal ferrite-martensite) because they are more susceptible to deformation hardening. The ferrite matrix contributes to good ductility, while the second phase (bainite, martensite and retained austenite) provides the high strength and high strain rate [111]. Other studies have focused on hardening mechanisms in Ti and low C microalloyed steels, using a combination of TMCP and ultra-fast cooling (UFC, 65 °C/s) [112]. This process improves the precipitation of carbides, nitrides with an average size smaller than 35 nm, and promotes the formation of martensite-austenite morphologies with 400 nm thickness, with yield strengths up to 650 MPa, and impact toughness of 93 J at −20 °C.

7. Microalloyed Steels Welding

Throughout history, multiple techniques for joining metals have been developed, all of them with different characteristics, advantages and defects. Among the most used today by the industrial sector are oxy-acetylene welding, electric arc welding, TIG (Tungsten Inert Gas) welding, MIG (Metal Inert Gas) welding, spot welding and the novel friction stir welding process (Figure 19), most of them used in different types of welding, such as circumferential welding joint (Figure 20).

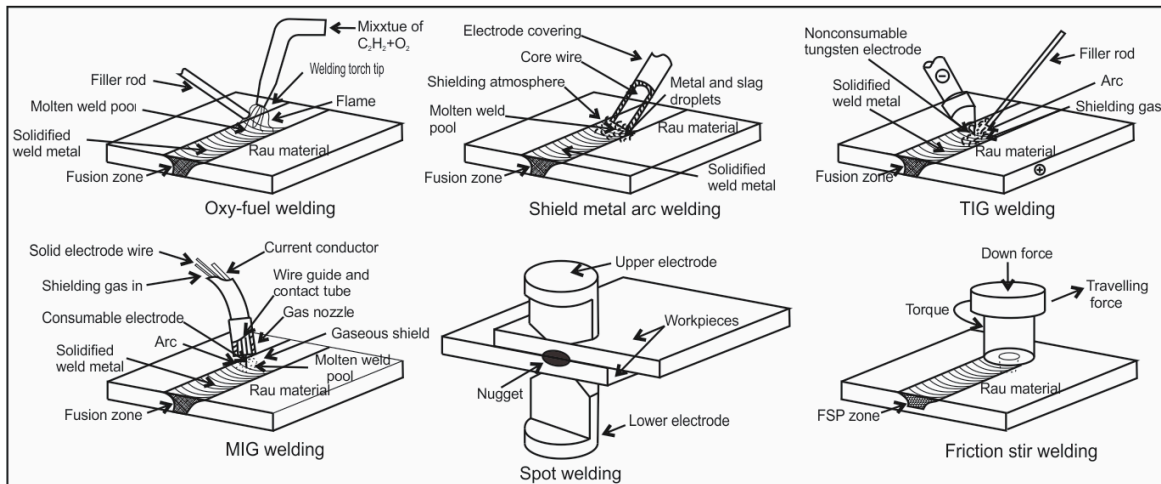


Figure 19. Most used types of welding processes.

All welding techniques modify to a greater or lesser extent the microstructure of the steels. The welding can be divided into zones: base metal (BM), heat affected zone (HAZ), partially melted region, interface, and weld metal (WM). In Figure 21, these zones are represented schematically. Figure 22 shows micrographs in optical microscope (Figure 22a) and scanning electron microscope (SEM) in the areas WM (Figure 22a,b), MB (Figure 22c) and HAZ (Figure 22d).

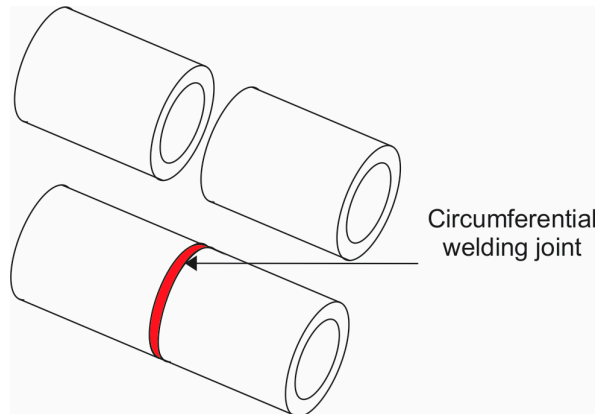


Figure 20. Circumferential welding joint.

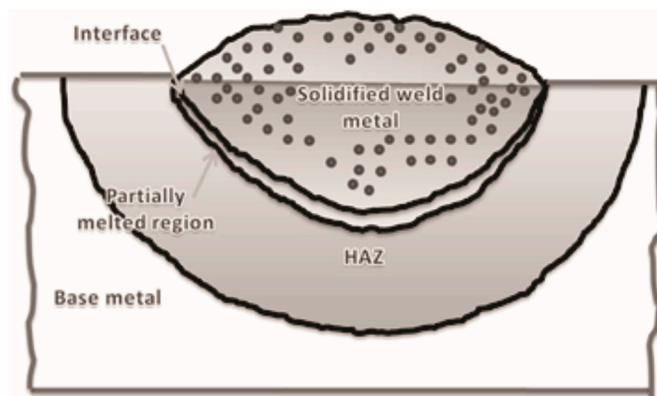


Figure 21. Schematic of welding regions.

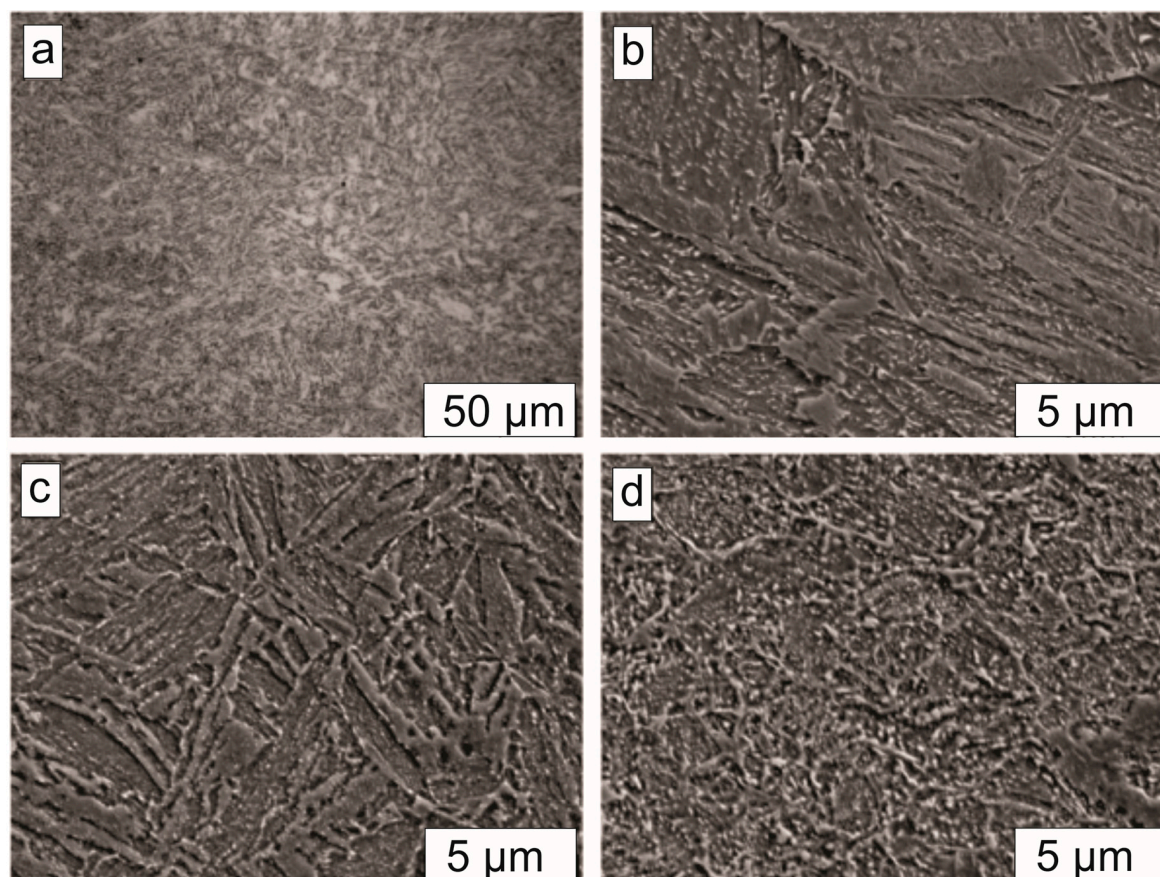


Figure 22. Optical (a) and SEM images of the WM (a,b), BM (c) and HAZ (d).

HSLA steels have been widely used for their excellent properties obtained through their microstructure, which is strongly altered by the selection of alloying elements and thermomechanical processes. [113]. In the year 2007, Bose-Filho et al. studied the effect of Ti, Ni, Mo and Cr on the microstructural development in the welding of an HSLA steel and reported that increasing the Ti content from 50 to 400 ppm does not contribute considerably to microstructural development; however, by increasing the content of Ni, Mo and Cr to increase the hardenability, they observed a change in the microstructural morphology from a mixture of allotriomorphic ferrite, Widmanstätten ferrite, acicular ferrite and microphases to a mixture of acicular ferrite, bainite, low carbon martensite and microphases [114].

Currently, the industry requires steels with high strength and toughness, and one of the ways to achieve this is through microalloy elements such as Ti. Studies have been carried out on steels with different Ti contents, and it was found that, in the fusion zone, Ti forms nano-sized carbonitrides that facilitate the formation of acicular ferrite due to a low energy interface of inclusion/matrix and the depletion of C in austenite during nucleation. The main cause of martensite formation is due to local C enrichment [115].

Bailey and Jones conducted a systematic study on the compositional variables on solidification cracking for submerged electric arc welding [116]. They incorporated a formula for obtaining crack susceptibility in terms of units of crack susceptibility (UCS), in function of the composition of the welded metal:

$$\text{UCS} = 230 \text{ C} + 190 \text{ S} + 75 \text{ P} + 45 \text{ Nb} - 12.3 \text{ Si} - 5.4 \text{ Mn} - 1$$

This formula is valid in the following composition ranges:

0.08–0.23% C	0.010–0.050% S	0.010–0.045% P	0.15–0.65% Si	0.45–1.6 Mn	0–0.07% Nb
--------------	----------------	----------------	---------------	-------------	------------

They concluded that there is no risk of cracking in compositions above the following compositions:

1% Ni	0.5% Cr	0.4% Mo	0.07% V	0.3% Cu	0.02% Ti	0.03% Al	0.002% B
-------	---------	---------	---------	---------	----------	----------	----------

In another study, it is indicated that adding V in pipes welded by submerged arc with 0.16% C and 1.4% Mn reduces the risk of solidification cracking [117].

The microstructure developed during the solidification of the welding pool highly relates to the obtained mechanical properties of the metals that have been fused using the welding technique. The union of HSLA steels tends to occur due to fracture toughness defects associated with the HAZ, and some of the problems in the HAZ have been reported, such as grain growth, formation of fragile phases close to the melting line, non-metallic inclusions and excessive softening [118,119]. Many studies have been carried out in order to minimize these defects. One of the techniques that has been studied is the application of an electromagnetic field (electromagnetic stirring), which prevents the deflection of the electrode and the electric arc during the welding process. By means of electromagnetic agitation, the formation of acicular ferrite during solidification is propitiated, which reduces epitaxial and columnar growth [120].

The grain growth in the HAZ is highly dependent on the stability of the nitrides during the thermal cycles of the weld. Loberg et al. have found that only TiN remains stable during the high temperatures present in the welding process. The best characteristics of fracture toughness and grain growth were obtained for optimal ratios of Ti/V/N with low Al levels [121].

For the determination of the kinetic parameters in the welding area, techniques such as synchrotron-based spatially resolved X-ray diffraction (SRXRD) can be used. Zhang, Elmer and DebRoy studied the welding of AISI 1005 steel during gas tungsten arc (GTA) welding using the SRXRD technique and found that over time there was a decrease in nucleation rate of austenite from a ferrite matrix [122].

Many studies have been carried out to determine the characteristics and formation conditions of acicular ferrite in welded steel, and some of the techniques used have been the computer-aided three-dimensional reconstruction technique and electron backscattered diffraction analysis. It has been observed that the acicular ferrite laths are formed by multiple nucleations in inclusions mainly formed by Ti, Al, Si, Mn and O and by sympathetic nucleation. The elongation of acicular ferrite takes place mainly in the early stages of grain formation, while the extensive hard impingement and mutual intersection are presented in the last stages of formation [123].

Recently, the techniques to improve fracture toughness in the HAZ have been studied extensively. The proposed methods usually focus on reducing the C content to avoid the formation of martensite–austenite in the HAZ and to add elements such as Ti, Zr and Ca to the alloy, in order to form fine oxide inclusions with high melting points that inhibit the thickening of austenitic grain [124–128]. The change in the microstructure in the HAZ due to thermal cycles derived from the welding process are the cause of a decrease in fracture toughness in localized areas, known as local brittle zones, coarse grained heat affected zone (CGHAZ) and intercritically reheated CGHAZ (ICCGHAZ) [129,130]. Lan et al. investigated the relationship between the fracture toughness and the microstructure of CGHAZ in low carbon bainitic steel. They reported a change from lath martensite to coarse bainite with the increase in welding cooling time, decrease in fracture toughness in cooling ranges between 10 and 50 s and an even a greater decrease when cooling times of 90 s or greater were used [131].

Another way of controlling the microstructure in the HAZ is through the selection of welding parameters such as current. It has been shown that, by changing the current intensity during welding, the hardness and tensile strength are changed [132]. The increase in current intensity causes an increase in the welding temperature, which increases the area of the HAZ, in addition to a change in the microstructure. In general, it is possible that, by increasing the current intensity, an increase of widmanstatten ferrite or martensite structures take place in the center of the weld due to higher cooling rates [133].

One of the methods that has been studied for the determination of the rate of transformation of phases on microalloyed steels has been the quantitative determination of the kinetics of the phase

transformation during welding by combination of mapping using X-ray diffraction and numerical modeling of the transport phenomenon [134].

In addition to the control of the microstructure through the selection of welding parameters, mechanical properties can also be controlled by another important parameter, such as protective gas. The variation of the protective gas composition can improve or decrease the final mechanical properties of the weld. Ekici et al. studied the mechanical properties in the welding of microalloyed steel, where they modify the composition of the protective gas. They used three compositions: 100% argon, a mixture of 15% CO₂ and 85% argon, and a mixture of 25% CO₂ and 75% argon. The welding was carried out using two techniques: gas metal arc welding (GMAW) and electric arc welding. They used two types of filler cables: coded as ER 100 SG and SG3 (G4Si1). They concluded in their article that the highest values of strength, hardness and ductility were obtained with the combination of 15% of CO₂ and 85% of argon using the filling cable ER 100 SG by means of the GMAW welding technique. They determined that electric arc welding can cause faults such as gas hole and slag formation. In addition, the mechanical properties obtained by this welding technique are lower [135]. By controlling the cooling time, the mechanical properties can be controlled. Dunder et al. determined that, for weld cooling times of 800–500 °C for 8–10 s in a microalloyed steel with increased resistance TStE 420, a decrease in the hardness of the HAZ is observed. In addition, the reduction of the risk of cold cracks and the values of impact toughness are increased [136].

The selection of the filling material also plays a very important role, since different compositions will generate different properties. Sharma and Shahi conducted a study on quenched and tempered low alloy abrasion resistant steels, which were welded using two types of austenitic stainless steel fillers. They found that by using fillers containing Cr and Mo with Nb, Ti, Al, V, Cu and N as microalloying additions, it resulted in martensitic refinement in the weld metal, which showed a microhardness of more than 400 HV as well as the percentage of elongation being reduced and its UTS increased displaying the highest joint efficiency [137].

One of the most recent techniques of welding is friction stir welding (FSW), which has great relevance in the industry because it has the potential ability to join dissimilar materials. Recent studies have focused on improving the properties of this technique, seeking a better appearance and defect-free joints [138]. The appearance of the weld and the reduction of the defects can be controlled by the tool rotation rate. Liu et al. studied the parameters involved to improve the welding of aluminum alloy with copper and determined that the best appearance was obtained under the condition of tool rotation rate of 600 or 1000 rev min⁻¹, welding speed of 100 mm min⁻¹, tool offset of zero and Cu sheet on the AS [138]. In Figure 23, an example of a weld with defects and poor appearance (Figure 23a) and a defectless weld with good appearance can be seen (Figure 23b).



Figure 23. Comparison between a weld with defects (a) and one without defects (b).

Among the problems associated with welding is HAZ hydrogen cracking, which is highly relevant in oil-gas pipelines failures. One of the factors that has been found to have some adverse influence on

the HAZ hydrogen cracking is the presence of V in the alloy, although, on the other hand, a more recent study in steel with 0.18% V showed that it is not necessary to include this element in the alloy [139].

Possible trapping sites in the weld metal are shown in Figure 24. The coexistence of the retained martensite and the carbides causes sites of hydrogen entrapment in the spaces between the acicular ferrites, since they have retained austenite and many interfaces causing the phenomenon of HAZ hydrogen cracking [140].

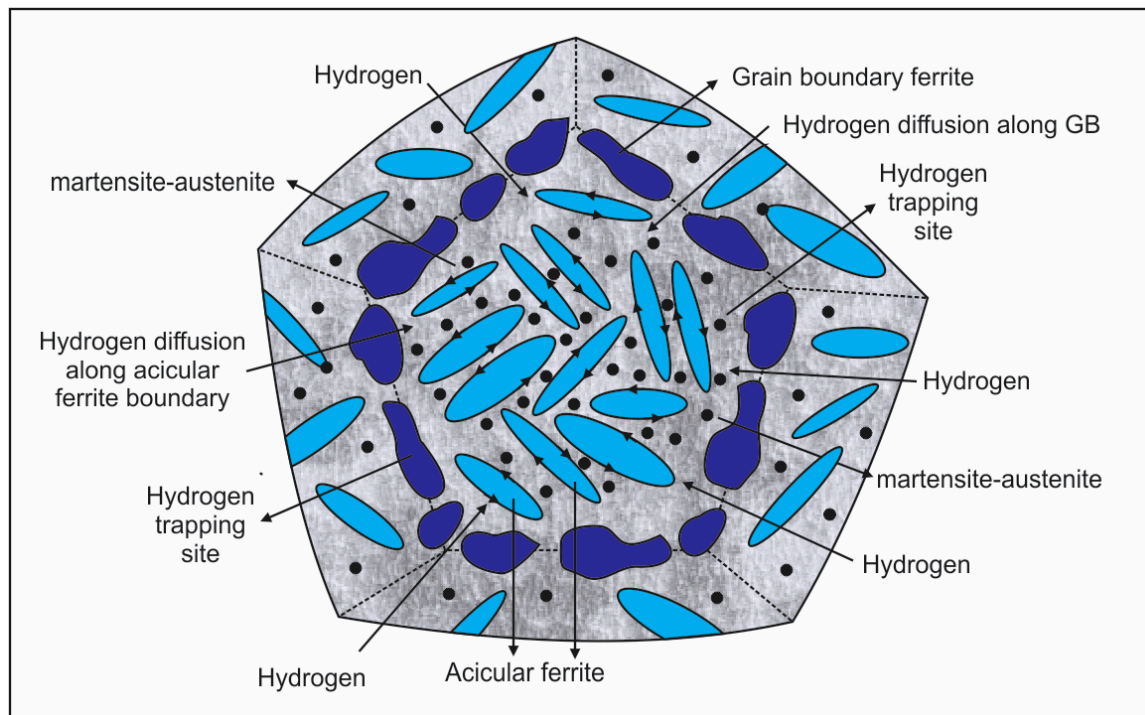


Figure 24. Schematic diagram of the hydrogen trapping sites in the weld metal [140].

In a study carried out by Hart and Harrison to determine the critical cooling times to avoid HAZ cracking, it was determined that these are related to the composition of the steel by the expression [139]:

$$\log \Delta t_{800-500\text{ }^{\circ}\text{C}}(\text{crit}) = 3.7 \left(C + \frac{\text{Mn}}{13} + \frac{\text{V}}{6} + \frac{\text{Ni}}{40} + \frac{\text{Mo}}{10} \right) - 0.31$$

Mechanical properties obtained in different welding zones are a function of microstructure. One of the most used techniques to know the mechanical properties in the welding zone is the determination of the microhardness by microindentation, which is under the “Standard Test Method for Microindentation Hardness of Materials” ASTM E384. Figure 25a shows the micrograph of a welded sample in which the microindentation was made. In Figure 25b the weld pool area is seen, in Figure 25c,d, the transition zones 1 and 2 are appreciated, and Figure 25e shows the heat affected zone.

Figure 26 shows the microhardness distribution as a function of distance from the welding center line. The tests were carried out at 2 mm distance from the top surface of the weld joints. The average microhardness of FZ (fusion zone), HAZ and BM was 356 HV, 325 HV and 298 HV, respectively (Table 7). These values correspond to the microhardness obtained in bainite and acicular ferrite morphology. FZ presented a higher microhardness due to its microstructure that consists of lath martensite. Wang et al [141] concluded that microalloying elements such as Cu, Ni and Cr could be dissolved in martensite causing an increment in microhardness [142]. The microstructure in HAZ zone consists of ferrite and martensitic microconstituents, and the content of lath martensite was decreased

but granular bainite increased gradually causing a reduction in microhardness. The microstructure and grain size are the most significant parameters that affect microhardness. Generally, the microhardness follows the relationship: martensite > bainite > perlite > ferrite [143]. The microhardness of the lath martensite and granular bainite was more than that of the ferrite, which resulted in a higher microhardness value in HAZ than in the BM.

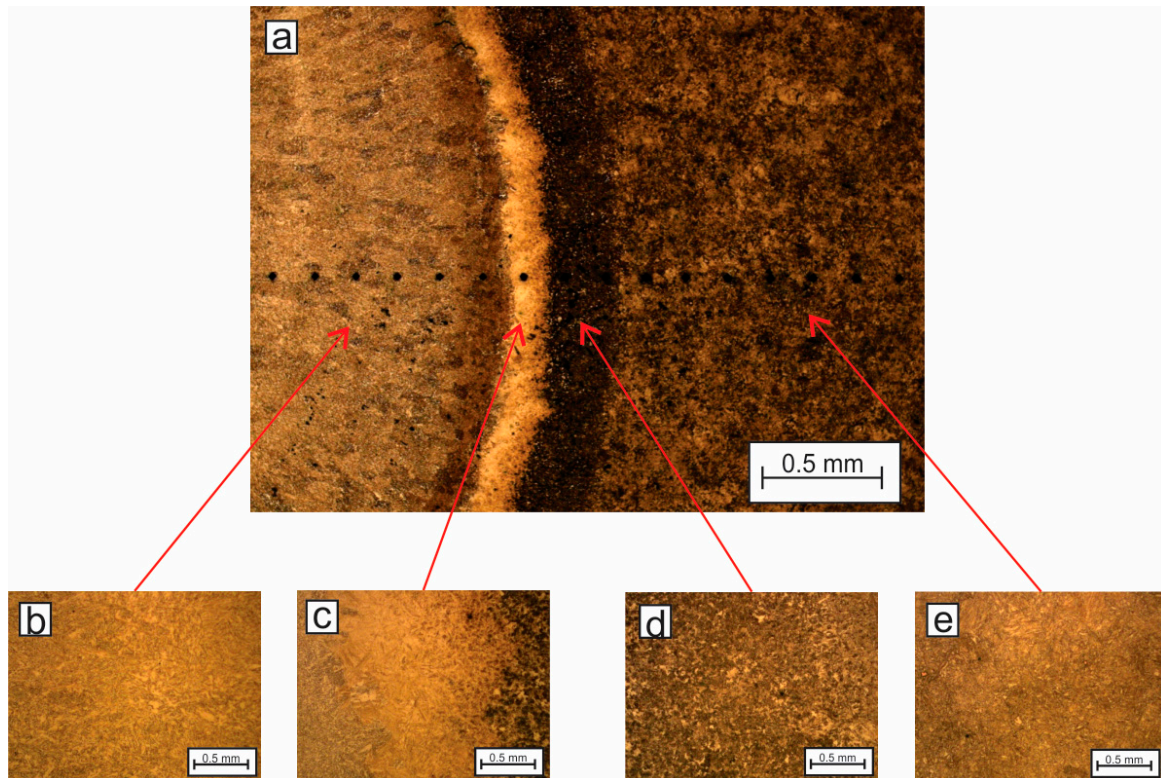


Figure 25. (a) Micrograph of a welded zone, (b) weld pool area, (c) and (d) transition zones 1 and 2, and (e) heat affected zone.

YS and UTS tend to decrease across the weld metal to the base metal, due to the variation in volume fraction of different ferritic morphologies and grain size. The temperature increment during welding, increases the diffusion rate causing that ferrite nucleates at austenite grain boundaries. As the temperature decreases in the weld pool, a ferrite transformation occurs and the grain boundary ferrite growth is suppressed; meanwhile, the acicular ferrite is produced in the austenite-acicular ferrite interface [144]; this causes acicular ferrite fine grains that reduce the strength and increase the toughness by inhibiting the interlocking mechanisms.

Bainite microstructure presents higher strength and lower ductility due to the high-density dislocations formed by accelerated cooling rate in weld metals that can produce acicular ferrite microphases [145]. The fine austenite grain size in HAZ contributes to the nucleation of bainite in the form of sheaves of small platelets [146]. The transformation of HAZ depends principally on two factors: a low transformation austenite-ferrite temperature during reheating that causes a complete austenite transformation, and high hardenability that allows a complete transformation into a mixture of acicular ferrite and bainite that have a good combination of mechanical properties [146].

Table 7. Average microhardness for different welding zones.

Welding Zone	Microhardness (HV)
Fusion zone	356
Heat affected zone	325
Base metal	298

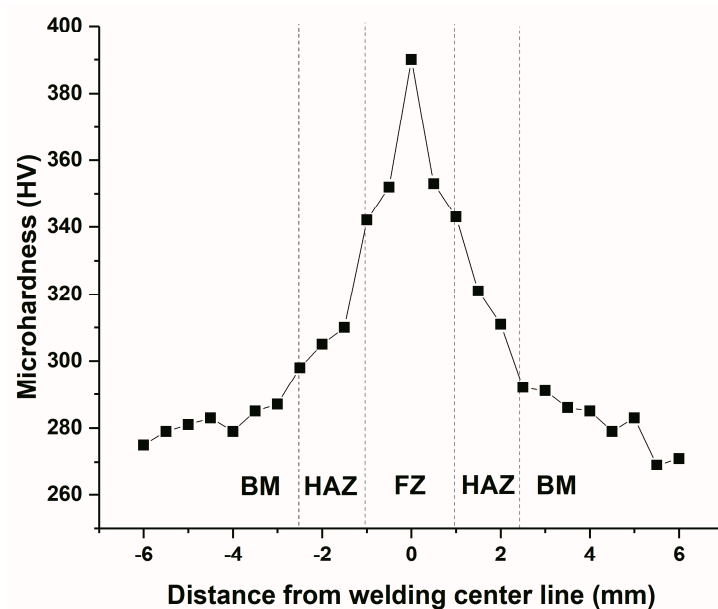


Figure 26. Microhardness profile as a function of distance from welding center line.

8. Hydrogen Embrittlement

Microalloy steels have been widely used in the hydrocarbon delivery industry, through the use of long-distance pipelines since their implementation in 1959 [147], due to their chemical composition and microstructures generated during their processing. These steels provide a good combination of mechanical properties such as high strength, toughness and good weldability, being some of the most economical options for the transport of natural gas. In the last two decades, microalloyed steels standardized by the American Petroleum Institute (API) have been used, the most common being the API 5L X-70, X-80 steels and recently the X-100 and X-120 steels [148]. With the growth of the petroleum industry, the oil-gas pipelines have been rapidly improved in terms of safety, economy and efficiency. With the increase of gas pressure, high strength pipeline steels are being widely used in various projects [80]. There are many applications in which the yielding stress of a material is a limiting factor in the design. If the strength of the material is increased, this would allow a structure to be lighter. Thus, the materials would offer a high resistance-weight ratio [87] and the pipeline wall thicknesses can be reduced, thus decreasing the production costs. Steels can be produced with yield stresses of up to 2000 MPa, but unfortunately as the yield stress is increased, other mechanical properties tend to decrease [149]. In general, materials become more susceptible to brittle fracture, especially when they are affected by ambient phenomena such as: hydrogen embrittlement, stress corrosion cracking (SCC), or corrosion-fatigue.

Hydrogen is a common element in the oil industry that can be generated as a corrosion by-product or by the application of welding with coated electrodes in the fitting of pipelines or valves. Variables such as: microstructure, strength, dislocation-recovery and carbide nano-coprecipitation can be very important for the hydrogen effects over the steel mechanical properties. These phenomena are associated with the amount of hydrogen absorbed by the steel, and its accumulation in the lattice and other defects; it enhances cracking, blistering and further failure.

The hydrogen embrittlement effects are characterized by a slight descent in the ductility up to a brittle fracture with a relatively low applied stress, ($\langle\sigma_y\rangle$) [150]. Even a few ppm of hydrogen dissolved in the steel can bring about cracking and loss of ductility, particularly in high strength steels. Few studies of the combined effects of microalloyed steels thermomechanically processed and hydrogen embrittlement susceptibility modify the mechanical properties—accomplished due to the hydrogen rate diffusion, trap site density and the exposed stress level in the presence of hydrogen, giving rise to local concentration of segregated hydrogen in tri-axial strain fields or on strain-induced defects.

Problems related to the formation of hydrogen-induced blisters tend to be more of a problem in low-strength steels used for pipelines intended for the transport of crude oil.

It is now established that high strength steels are susceptible to embrittlement by hydrogen dissolution and mainly to failure by SCC cracking attributed to hydrogen embrittlement [151]. There are two main classes of hydrogen effects:

- Quasi-brittle fracture in high strength materials that can occur with relatively low concentrations of hydrogen.
- Internal cracking and surface blistering in low strength materials (mainly C steels) due to very high internal hydrogen fugacity, allowing hydrogen pressure induced cracking, commonly referred to as HIC.

X80 pipeline steel, as high strength pipeline steel, is becoming one of the most widely applied pipe materials because of its high strength and toughness, which not only saves lots of steel, but also has a better performance [92]. However, hydrogen induced cracking (HIC) has been acknowledged as one of the predominant failures in pipeline steel in humid environments with H_2S and other sour materials, which causes the heavy leakage of oil as well as serious economic losses and casualties [152].

Up to now, a lot of work has been done to investigate the properties of X80 pipeline steel. Hardie et al. [153] compared the susceptibility to hydrogen embrittlement of three kinds of API pipeline steels (X-60, X-80, and X-100 grades), showing that the increase of strength level tends to decrease the resistance of steels to HIC. Shin et al. [154] studied the relationship between the microstructure and Charpy impact properties of X-70 and X-80 pipeline steels. Shterenlikht et al. [155] reported the capacity of the anti-ductile crack growth of X-80 pipeline steels. Kong et al. [105] reported the effect of Mo on the microstructure and mechanical properties of X-80 pipeline steel. However, the specifics for HIC of X-80 pipeline steel, and additionally the impact of inclusions on HIC and the mechanical properties of the steel are still unknown. In view of this, it is extremely necessary to work out the details of hydrogen-induced damage and how these failures deteriorate the properties of X-80 pipeline. Hydrogen induced cracking in X-80 pipeline steel under various electrochemical hydrogen-charging conditions as well as the influence of inclusions and microstructure on the origin of HIC were investigated in this work.

Reversible hydrogen embrittlement can occur after small concentrations have been absorbed from the environment. However, local concentrations of hydrogen may be larger than the average values because the absorbed hydrogen diffuses between the grains or preferably at the grain boundaries. The hydrogen embrittlement is affected by the rate of deformation, which suggests that diffusion is time dependent as a control factor. On the other hand, embrittlement is more severe at room temperature during sustained stress or in tests conducted at slow deformation rates. Another factor such as elevated temperatures can cause hydrogen to diffuse in areas of concentration. The effect of hydrogen is also strongly influenced by other variables, such as (Figure 27):

- The level of stress (or hardness) of the alloy;
- The microstructure;
- The amount of stress applied;
- The presence of localized tri-axial stress;
- The previous amount of cold work;

- The degree of stress segregation of low melting point elements such as: P, S, N, Ti or Sb at the grain boundaries.

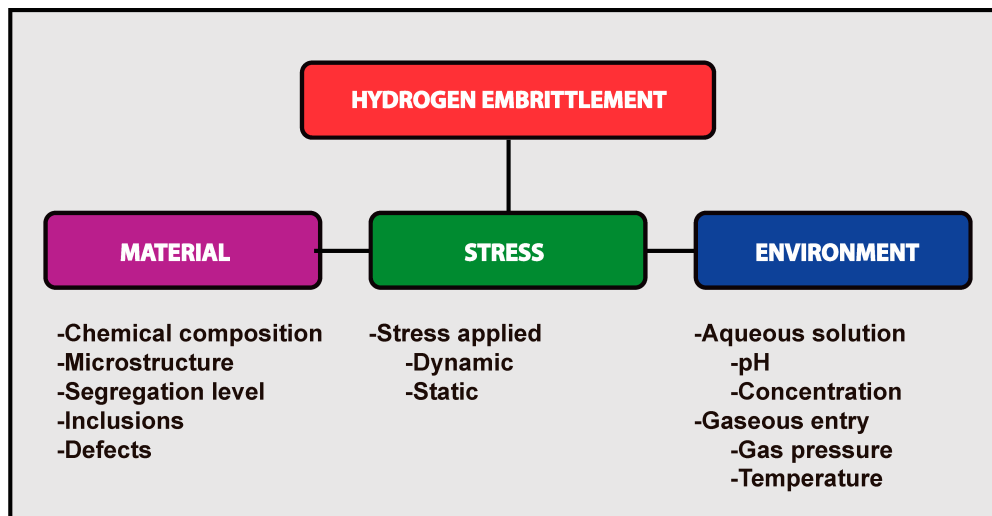


Figure 27. Principal variables involved in the hydrogen embrittlement phenomenon [156].

8.1. Hydrogen Trapping

The hydrogen absorbed in the steel can exist in different forms, mainly monoatomic:

- Interstitial hydrogen, dissolved in solid solution in the steel matrix.
- Hydrogen associated with structural defects, such as dislocations or second phase particles.
- Hydrogen accumulated in voids or blisters in gaseous form.

These different forms present different mobility and solubility in the crystalline structure of the steel, which affects the mechanical properties to different degrees. Hydrogen atoms are strongly attracted to defects in metals; these are referred to as hydrogen traps [157]. These traps include vacancies, dislocations, grain boundaries, second-phase particles and non-metallic particles [152].

Hydrogen traps are commonly characterized as irreversible or reversible [158] and are related to the number of hydrogen atoms that can be retained. The influence of each trapping site will depend on its density and its activation energy. Irreversible traps are those sites with high activation energy, and where the residence time of hydrogen is higher; hydrogen is usually regarded as non-diffusible. On the other hand, hydrogen trapping sites with low activation energy are considered as reversible traps, in which case the hydrogen will have higher diffusivity [159].

Trapping sites may be generated and/or modified during thermal and mechanical processes due to the kinetics of second phase particle precipitation, inclusions distribution, dislocation density, grain size change, dimple formation and microcracks [160,161]. According to Liu et al. [162], reversible traps may have a greater influence on the diffusion of hydrogen and the susceptibility to embrittlement, since the residence time of the hydrogen atoms is smaller, leading to high diffusivity. Hirth [163] suggested that a material with finely distributed irreversible traps is less susceptible to hydrogen embrittlement.

The segregation of C, form and distribution of precipitates (Nb, V, Ti) (C, N), as well as other nonmetallic impurities may increase hydrogen trapping. Some studies have concluded that carbide interfaces and the presence of incoherent precipitates, present higher trapping energy compared to grain boundaries and dislocations [164]. However, the latter play an important role in mechanisms of hydrogen embrittlement [165]. Wei et al. [166] studied the influence of TiC precipitates coherence and observed that coherent and semi-coherent precipitates of TiC showed a considerable difference in their trapping energy (55.8 kJ/mol), as well as in the activation energy to release hydrogen

(95 kJ/mol), concluding that the activation energy in this type of precipitate is smaller and therefore behaves as reversible traps. Escobar et al. [167] observed a similar behavior, and the activation energy of semiconducting TiC precipitates is lower than the incoherent particles. On the other hand, Wallaert et al. [168] has reported that (Nb) (C, N) tend to form irreversible traps. However, Takahashi et al. [169] reported that fine coherent TiC particles smaller than 10 nm were the most effective sites for entrapment and Valentini et al. [170] observed that Ti (C, N) precipitates less than 35 nm were the strongest irreversible traps in microalloyed steels.

This susceptibility to hydrogen embrittlement will depend on the entrapment and release kinetics of hydrogen in the crystalline defects, directly influencing the rate of diffusion and the concentration of hydrogen in the steel. McNabb–Foster models [171] have been developed to determine this behavior.

8.2. Hydrogen Embrittlement Mechanisms

Hydrogen embrittlement is a complex phenomenon manifested in various forms. This is caused by the presence of small amounts of hydrogen, triggering catastrophic failure due to residual stresses or by applying relatively small loads, causing degradation in ductility or toughness [172]. Many mechanisms have been proposed; however, the following are considered the most common [165,173]:

- (1) Hydrogen enhanced decohesion (HEDE). This mechanism proposes that hydrogen causes a reduction in the bond strength of metallic atoms, allowing weakness under tensile loads, in addition to promoting a propagation of fragile cracks [174].
- (2) Hydrogen enhanced local plasticity (HELP). This mechanism proposes that the presence of hydrogen increases the mobility of dislocations, causing a highly localized plastic deformation [175]. Because this deformation is concentrated in a small volume, the macroscopic ductility is low.
- (3) Absorption induced dislocation emission (AIDE). This mechanism is very similar to the HELP mechanism because it also involves localized plasticity. However, the main difference is that the AIDE mechanism proposes that localized plasticity occurs close to the surface in regions of stress concentration, such as cracks [176]. The hydrogen causes the movement of dislocations towards the crack tips, causing the growth of the same, as well as an intense deformation in the vicinity of the crack.

Depending on the interaction of the hydrogen with the dislocations (during the deformation processes), the movement of dislocations can be promoted, inducing a localized plasticity. In addition, the dislocations are accumulated in microcracks, causing their subsequent propagation [177]. On the other hand, during the plastic deformation processes, the movement of dislocations can cause trapped hydrogen to diffuse to zones of higher stress intensity crack points, causing their recombination in molecular hydrogen, causing blistering and increasing their local concentration [153]. This significantly affects the performance of the steels under mechanical load and the type of fracture prevalent during failure.

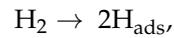
8.3. Hydrogen Entry

Hydrogen can enter the metals in gaseous form or by an electrochemical reduction of the hydrogen-containing species of aqueous phases. This process depends on many parameters and is the first step for the development of hydrogen embrittlement. For the first case, these factors are mainly environmental, such as applied pressure, gas purity and temperature; meanwhile, for the second case, the predominant factors are the potential of the electrolyte-metal interface, the applied current density, the electrolyte composition and the pH of the solution [178].

8.4. Hydrogen Gaseous Entry

Many models have been proposed for the hydrogen gaseous entry, and the details of this process are still uncertain. In general terms, however, the reactions involved are adsorption of molecular

hydrogen, dissociation of the hydrogen molecule and thus hydrogen atoms are adsorbed on the surface, and the subsequent diffusion of atoms adsorbed on the surface within the crystal lattice of the metal [179]:



For most metals exposed to gaseous hydrogen atmosphere, the gas–solid interaction is defined by three steps: physisorption, chemisorption and absorption [180], these processes are depicted in the Figure 28.

- Physisorption: is the result of Van Der Waals forces between the metal surface and an adsorbent. It is completely reversible, and usually occurs instantly (direct adsorption of the hydrogen molecule on the surface).
- Chemisorption: is a chemical reaction that occurs between an atom of the metal surface and the adsorbent molecule. The chemical forces involved are short range and are limited to single layers. Chemisorption is usually slow and may be slowly reversible or irreversible. This process may be related to the formation of covalent bonds between an atom or adsorbent molecule and a surface atom (direct dissociation to atomic hydrogen).
- Absorption: it is a gas–solid interaction, which involves the incorporation of the products of the chemisorption within the crystalline network of the steel and its subsequent diffusion. Depending on the input mechanism, hydrogen absorption may be in atomic or ionic form (H^+) [181].

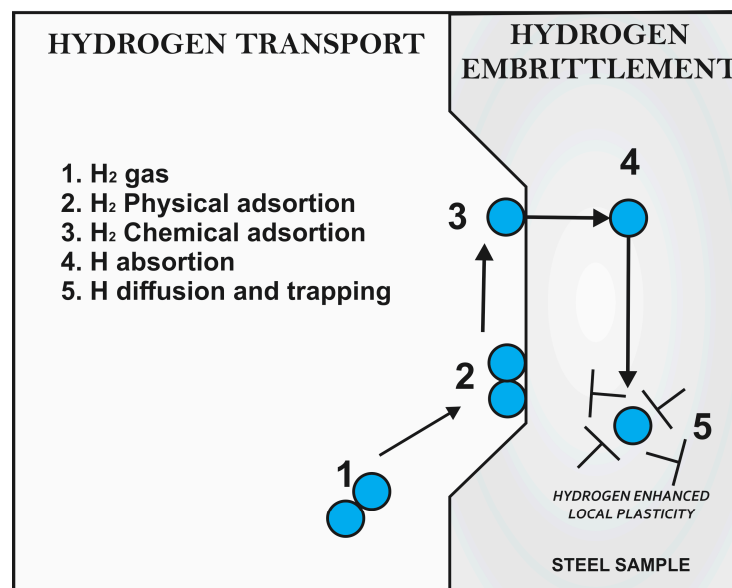


Figure 28. Hydrogen gas entry mechanism in metals.

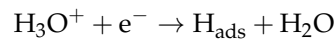
The hydrogen embrittlement effect is strongly affected by environmental factors such as hydrogen gas pressure, hydrogen purity and temperature. The HE susceptibility at high pressure (70 MPa) is influenced by hydrogen solubility (S) and diffusivity (D). The S are a function of hydrogen surface concentration (C_0) and hydrogen pressure (P) according to the Sievert's law [182]:

$$C_0 = SP^{1/2}$$

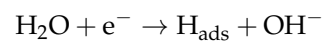
Due to the direct relation between C_0 and P applied, the increment of gas pressure is related to high hydrogen embrittlement susceptibility [183]. That is, ductility tends to reduce proportionally to the square root of hydrogen pressure [184].

8.5. Entry of Hydrogen into Aqueous Phase

The mechanism of electrochemical production of hydrogen in steels in aqueous solution has received much attention. It is accepted that the reaction occurs in several stages. The first of these is an initial charge transfer that produces adsorption of the atomic hydrogen. In acid solutions, this involves the reduction of a hydrogen ion:



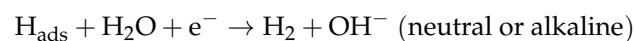
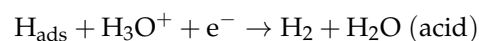
In neutral and alkaline solutions, where the hydrogen concentration is very low, the reaction changes for the reduction of the water molecules:



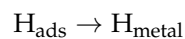
The second stage of the reaction to produce molecular hydrogen can occur through two mechanisms. In the first of these, known as chemical desorption, chemical recombination or Tafel reaction, two adsorbed hydrogen atoms combine to produce molecular hydrogen:



Alternatively, adsorbed hydrogen atoms may participate in a second electrochemical reaction, known as electrochemical desorption, or Heyrovsky reaction [151]:



A third reaction, which goes in parallel with the desorption reaction, is the entry of the atomic hydrogen into the metal from a surface adsorption state:



In many circumstances, the kinetics of these reactions are controlled by the rate at which hydrogen can diffuse into the metal.

If the adsorbed hydrogen is produced from a gas phase or an aqueous solution, it appears that the presence of the hydrogen atoms distorts the crystal structure of the metal surface [185].

In Figure 29, it is shown a hydrogen charging cell using 0.5 M H_2SO_4 + 0.2 gr As_2O_3 .

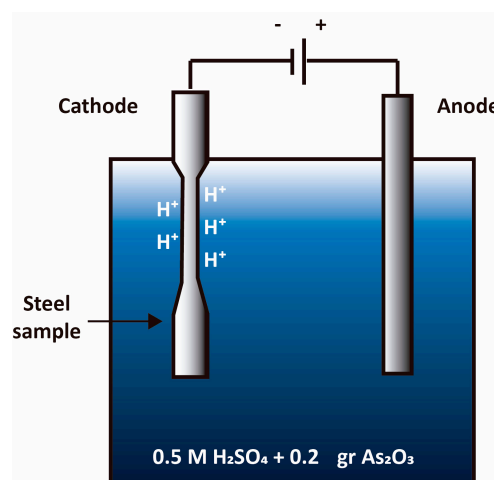


Figure 29. Hydrogen charging in a 0.5 M H_2SO_4 + 0.2 gr As_2O_3 .

8.6. Hydrogen Embrittlement Effect over Mechanical Properties of Tempered Treated Microalloyed Steels

The HSLA steels are used for hydrogen storage and transportation, due to their high strength, toughness and good weldability. These steels are subjected during its processing to thermomechanical processing (TMCP), as well as heat treatment to adjust the final mechanical properties [186,187]. The TMCP is an important aspect in the production of API grade steels, parameters such as reheated temperature, rolling temperature and cooling rates play a significant role in the obtainment of final microstructure and mechanical properties [188]. The Nb addition as a microalloying element tends to refine the austenite grain size [189], obtaining banded ferrite–perlite microstructures if fast cooling after controlled rolling is not applied.

Zhou [190] studied the mechanical properties on microalloyed steels as a function of its obtained microstructures through different thermo-mechanical processes that consisted of direct quenching and a posterior tempering at 500 °C for 1 h. They studied the mechanical properties of these steels in relation to their microstructure, which was obtained by different thermo-mechanical processes consisting of direct annealing and tempering at 500 °C for 1 h after the process controlled rolling mill (DQT); and direct annealing, annealing and subsequent quenching and tempering (RQT), obtaining microstructures of deformed bands of retained austenite and martensite; in addition, by means of a second thermo-mechanical treatment, a typical martensite microstructure is obtained in the form of needles without deformed bands. When this microstructure is precipitated, the precipitated carbides grow at the borders of the martensite needles; some of the precipitates have been identified as (Nb, Ti) (C, N) by EDS (Energy Dispersive Spectrometry). These studies conclude that, as the tempering temperature increases, the yield stress keeps fluctuating slightly near 1033 MPa, but the tensile stress decreases drastically, as well as an increase in the percentage of elongation of the material. The impact tests carried out indicate that higher tenacity values are achieved at tempering temperatures ranging from 500 to 650 °C in both types of microstructures [190].

Zhong Ping [191] evaluated the effect of heat treatment of tempering on the microstructure and mechanical properties of an ultra-high strength steel with a final tensile stress of 2230 MPa that is subjected to tempering thermal treatments during six hours in a temperature range of 100 °C to 650 °C. The effect of secondary hardening on tempering heat treatments over a range of temperatures resulted in a substantial change in mechanical properties particularly in impact toughness, fracture toughness, as well as an increase in yield stress and tensile strength in ranges from 300 °C to 480 °C; on the other hand, at 650 °C, the strength decreased, as well as also exhibiting lower tenacity properties at a range of 400–470 °C; nonetheless, this increased considerably at 510 °C. The optimum combination between strength and toughness is achieved in a temperature range of 480–510 °C. The results of the studies by TEM indicate that, in the early stages of tempering, the precipitates could be in the form of agglomerates; meanwhile, the increases of strength at 470 °C may be the result of a microstructure consisting of uniform dispersion, irregular shapes, coherent zones or carbides; however, at 510 °C, due to the loss of coherence in the precipitates, the strength decreased.

8.7. Hydrogen Embrittlement Effect over the Mechanical Properties

Microalloyed steels are intended to be used in the transportation of sour gas, since the extracted gas contains dissolved hydrogen sulfide (H₂S), the corrosion process in the pipelines is aggravated. Under these conditions, the cracking of these pipes is favored by the presence of atomic hydrogen produced on the surface as a corrosion byproduct of the exposed steel [192].

Microalloyed steels may fail due to severe H₂S degradation, which is present in crude oil and natural gas, so attention should be paid to the size, morphology and distribution of non-metallic inclusions in microalloyed steels to avoid hydrogen induced cracking (HIC), as well as the type of microstructure present in the steel and the strength level of the material.

The effect of material factors on the diffusivity of hydrogen depends on two main factors, which are: the concentration of atomic hydrogen on the metal surface due to environmental factors such as the pH of the solution and the partial pressure of hydrogen gas; the other factor is microstructural

consisting of primary and secondary phases including nonmetallic inclusions and precipitates that can affect the entrapment and diffusivity of the steel.

Some of the factors that can affect the mechanical properties of steels, and their effects are described below:

Elastic constants. There is evidence of small changes in the elastic properties of steels as a result of dissolved hydrogen. These changes are small and therefore impractical. This is perhaps from the point of view of the low hydrogen solubility in the iron crystal lattice and the small effect on the metal–metal bond strength [193].

Bonding effort. The effect on the yield stress of iron and steels is unpredictable. For pure iron, polycrystalline or monocrystalline, the yield stress frequently shows a decrease due to the effect of hydrogen but can be increased or maintained, depending on the dislocation structure, crystalline orientation and iron purity [193]. In the next picture (Figure 30), the hydrogen embrittlement effect on mechanical properties of API X-120 microalloyed steels are shown. Strength (Figure 30a,b) and strain fracture tend to decrease as hydrogen charging time increases, and the stiffness increases as time increases (Figure 30c). These results show the embrittlement effect of hydrogen and the detrimental effect on mechanical properties.

Plastic behavior. The effect of hydrogen on the plastic behavior of iron and steel is very complex, hydrogen can harden or soften the material, according to its structure and the slip mode. Lunarska [193] concluded that hydrogen segregation around dislocations reduced its elastic range. At room temperature (where the diffusion rate of hydrogen is sufficiently high that it can maintain the movement of dislocations), this allows a softening of monocrystals when only a sliding system is operative. Hydrogen can also suppress the slippage of screw dislocations, and this results in hardening when multiple slip systems are activated [151].

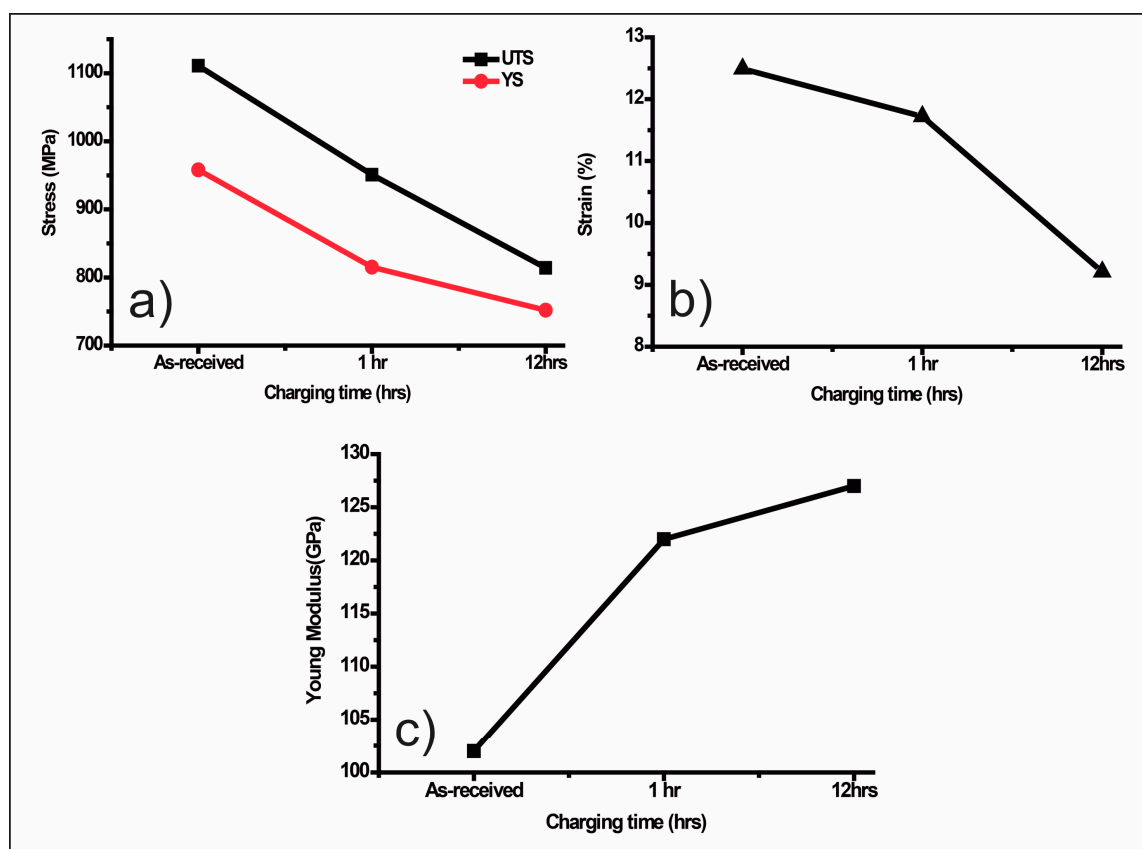


Figure 30. Hydrogen embrittlement effect, (a) UTS and YS, (b) strain percent and (c) young modulus; as a function of charging time.

In 2006, Hardie [153] carried out comparative studies on three different grade API steels of different resistance levels from the point of view of susceptibility to hydrogen embrittlement. The microstructure of these steels consists of bands of pearlite distributed in a ferrite phase in an elongated structure in the longitudinal direction to the rolling. The average grain sizes are 8, 4 and 2 μm , with microhardness of 200, 224 and 252 HV (Vickers Hardness) respectively. Some of their results show that there are different susceptibilities to the loss of ductility after a cathodic hydrogen charge and this susceptibility tends to increase with the resistance level of the steel when a current density of 0.44 mA/mm^2 is applied. Figure 31 shows the current density applied over area reduction in different API grade steels. These presented a significant loss of ductility when subjected to cathodic cracking, and the degree of embrittlement increased with the increase in current density, attributable to a higher uptake of hydrogen during this process.

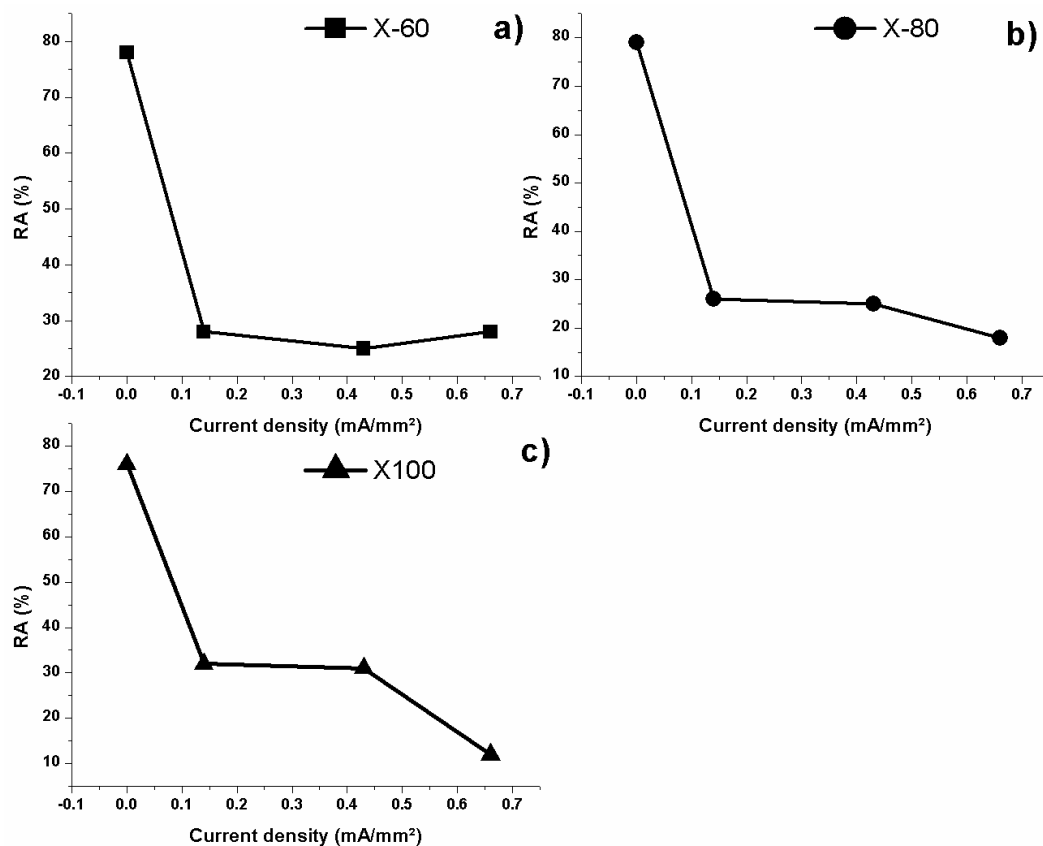


Figure 31. Reduction area change in different API grade steels. (a) X-60, (b) X-80 and (c) X-100, as a function of current density applied [153].

Other studies carried out by Gyu Tae Park [194] tried to evaluate the effect of the microstructure on the susceptibility to hydrogen embrittlement and compare the entrapment efficiency of hydrogen in microstructures consisting mainly of pearlite–ferrite, acicular ferrite, and ferrite–bainite; to evaluate the entrapment of hydrogen they calculated the permeability ($J_{ss}L$) and apparent diffusivity (D_{app}), where the entrapment efficiency of hydrogen increases in the following order of microstructures: perlite–ferrite, ferrite–bainite and acicular ferrite, the latter being the most susceptible to hydrogen embrittlement, as well as certain cracking initiation sites that are caused by nonmetallic inclusions, usually reported as crack initiation sites. As the microstructure changes from acicular to ferrite–bainite ferrite, the susceptibility to embrittlement by hydrogen increases, this being explained by the high tenacity of the acicular ferrite, preventing the propagation of cracks; low values of $J_{ss}L$ and D_{app} , and high values of C_{app} exhibit higher entrapment of hydrogen in the steel.

On the other hand, Liu et al. [195] evaluates the effect of microalloyed steel subjected to heat treatments consisting of air cooling to obtain a microstructure of bainite–martensite, which shows a superior combination of strength and toughness than when a martensitic microstructure is obtained from a quench and then tempered at intermediate temperature. It is concluded that the susceptibility to hydrogen embrittlement of steel with bainite–martensite microstructure decreased as the tempering temperature increased from 280 °C to 370 °C. The results show that the susceptibility to hydrogen embrittlement decreases as the tempering temperature increases, where, after 370 °C, the bainitic-martensitic microstructure is less susceptible to embrittlement. One reason is that area reduction (%RA) has greater stability after tempering at this temperature; another reason is that the internal stresses have been relieved.

Other studies indicate that the increase in the pre-charged time, the increase of the applied current density or the decrease of pH in the test solution allows the increase in the content of hydrogen in an API-X80 grade steel, and this promotes the reduction in the percentage of area reduction in stress tests and consequently a higher index of embrittlement by hydrogen.

Dong [196] studied the relationship between the microstructure and the Charpy impact properties in API grade X-70 and X-80 steels, using current densities of 20, 50 and 100 mA/cm² and times of 1, 3, 5 and 8 h exposure to an H₂SO₄ medium, where the mechanical properties of these steels are assessed by stress tests. It was found that there is a reduction in the strength of the material as well as a considerable decrease in elongation and reduction of area after longer exposure times. The fractographic study carried out showed a greater brittleness and cracking at the fracture surface with a longer pre-loading time. The type of fracture present shows evidence of a type of brittle fracture due to the presence of cleavage zones.

9. Future Trends

The growth of petroleum distribution systems has always been closely associated with the development of microalloyed steel grades having high strength, toughness, and weldability. In many ways, the research in microalloyed steel drew impetus from the huge demands of such steels from the petroleum pipeline projects. The first specification for steel for pipelines introduced by the American Petroleum Institute (API) in 1948 was X-42 with a yield strength of 42 ksi or 290 MPa. The strength levels underwent large scale changes over the decades, and, at the present time, the X-80 is a commonplace alloy, while X-100 and X-120 are still in sight. High temperature processes (HTP) are an important factor for consideration in pipelines development. The necessity of incorporating facilities for producing high-strength pipeline steels in up-coming steel plants has been briefly dealt with. With increasing strength levels in pipeline steels and higher operating pressures coming into vogue, pipeline steels emerge as a subject of fresh research, innovation, and area of specialization [197].

Today, heavy plates for longitudinally welded pipes in the X-80 strength grade are produced by Mannesmannröhren Mülheim (MRM) with the same reliability as lower grades [198].

The manufacturing of products with excellent quality is the ultimate goal of technological development. To achieve this goal, the properties of manufactured products must be predicted, and both the chemistry and the production process must be carefully designed. Recent advances in physical metallurgy, rolling technology and computer control have made great contributions to the field of structure and property prediction and to the development of a control model that allows the prediction of microstructural evolution and mechanical properties. It is expected that the maximum benefits from manufacturing control will be obtained by using predictions derived from metallurgical models [197].

Resource conservation, energy reduction, yield improvement, recycling and reduction in the weight of parts are becoming increasingly important. In the future, microstructure control will therefore be expected to assist in the development of new processing technologies that offer improvements in the above areas. One example of this is the manufacture of parts with high strength and good machinability. This kind of new technology will be applied to many microalloyed steels. It will prove

necessary to develop a precise system for the simulation of microstructural evolution during forming in order to optimize process design for these types of functional parts.

The Latin American steel industry continues its effort to modernize its facilities, including in the complicated context of the global situation generated by China's overcapacity and the government's subsidies to steel exports. A part of the modernization effort is reflected in the construction of new plants, which meets different needs.

A good part of these plants has been installed in the center and north of Mexico, primarily focusing on the strong development of the automotive industry, and its consequent exports to the USA. Another important part of the new plants corresponds to the states of Pará, Maranhão and Ceará, in the north and northeast of Brazil, where local governments have offered very favorable conditions for investments.

Innovative technologies are being introduced: the first Jumbo Coking Reactor (JCR) plant in the Americas; the world's first Quantum electric furnace; the first continuous casting of Castrip straps outside the USA and the first ecological pickling plant in Latin America (TYASA). One of the plants uses pig iron produced from biomass (Aço Verde Brasil).

The routes implemented range from electric steel mills that use scrap to integrated mills based on blast furnaces and oxygen mills, also including routes used only in Latin America, such as integrated blast furnace mills and charcoal mills in addition to plants included that are dedicated exclusively to cold rolling or hot dip galvanizing. One particular feature is the installation of flat-bed laminators in a single box, for relatively small production compared to conventional laminators (Gerdauro Branco, AHMSA, TYASA) [199].

At the moment, analytical techniques have been used, such as:

High resolution synchrotron X-ray experiments that can be carried out to accurately measure the NbC volume fraction and corresponding dissolved Nb in solution after reheating conditions, which is otherwise difficult to measure by electron microscopy or conventional X-ray diffraction because of very low volume fraction (about 0.0001–0.0002) of niobium carbide precipitates in the investigated alloys [200].

Hot compression experiments with variable strain and strain rates can be carried out to develop equations for recrystallization kinetics of deformed austenite in the investigated Nb-microalloyed rail steels. In addition, the effect of plane-strain compression and other complex deformation schedules on the recrystallization kinetics can be studied [201].

A more in-depth study of non-propagating secondary cracks in various pearlitic and bainitic microstructures would provide valuable insight and complement existing results [202].

The effect of Nb-microalloying on other important rail properties like rolling contact fatigue performance, weldability, hydrogen embrittlement, etc. needs to be investigated.

Author Contributions: S.S. and B.C. got the idea and directed the project and review of the final version; J.C.V., A.D.-P. and J.M. wrote the paper.

Acknowledgments: This work was supported by PRODEP [grant number 511-6/17-14378] and for the support in the payment of the costs of publication, CONACyT [grant number 434894]; we want to thank to Ben Church; René Guardian Tapia and Ivan Puente Lee for the support provided in SEM images and Alejandro Sedano Aguilar for the support in the revision of the English grammar of the article.

Conflicts of Interest: The authors declare no conflict of interest.

References

1. Stalheim, D.G.; Muralidharan, G. The Role of Continuous Cooling Transformation Diagrams in Material Design for High Strength Oil and Gas Transmission Pipeline Steels. In Proceedings of the IPC 2006, Calgary, AB, Canada, 25–29 September 2006.
2. Takahashi, A.; Lino, M. Thermo-mechanical control process as a tool to grain-refine the low manganese containing steel for sour service linepipe. *ISIJ Int.* **1996**, *36*, 235–240. [[CrossRef](#)]

3. Fu, J.; Wang, J.B.; Kang, Y.L. Research and development of HSLC steels produced by EAF-CSP technology. In Proceedings of the International Symposium on Thin Slab Casting and Rolling, Guangzhou, China, 3–5 December 2002.
4. Xu, G.; Gan, X.; Ma, G.; Luo, F.; Zou, H. The development of Ti-alloyed high strength microalloy steel. *Mater. Des.* **2010**, *31*, 2891–2896. [[CrossRef](#)]
5. Becket, F.M.; Russell, F. Steel. U.S. Patent 2,264,355, 2 December 1941.
6. Gray, J.M.; Siciliano, F. High Strength Microalloyed Linepipe: Half a Century of Evolution. In Proceedings of the Pipeline Technology Meeting, Houston, TX, USA, 22–23 April 2009.
7. Beiser, C.A. The Effect of Small Columbium Additions to semi-killed Medium-Carbon Steels. ASM Preprint No. 138. In Proceedings of the Regional Technical Meeting, Buffalo, NY, USA, 17–19 August 1959.
8. Morrison, W.B. The Influence of Small Niobium Additions on the Properties of Carbon-Manganese Steels. *ISIJ Int.* **1963**, *201*, 317.
9. Irani, J.J.; Burton, D.; Jones, J.D.; Rothwell, A.B. Beneficial Effects of Controlled Rolling in the Process of Structural Steels. In *Strong Tough Structural Steels*; Iron and Steel Institute Special Publication: Scarborough, UK, 1967.
10. Iron and Steel Institute. Strong Tough Structural Steel. In Proceedings of the Joint Conference, Scarborough, UK, 4–6 April 1967.
11. Cuddy, J.L. The Effect of Microalloy Concentration on the Recrystallisation of Austenite During Hot Deformation. In *Thermomechanical Processing of Microalloyed Austenite*; AIME: Pittsburgh, PA, USA, 1981; pp. 129–140.
12. Tata Steel. Available online: <http://www.tatasteeleurope.com> (accessed on 16 January 2018).
13. Starratt, F.W. Columbium-treated steels. *J. Met.* **1958**, *10*, 799.
14. Oakes, G.; Barraclough, K.C. *Steels; The Development of Gas Turbine Materials*; Applied Science Publishers: London, UK, 1981; pp. 31–61.
15. Llewellyn, D.T. Nitrogen in steels. *Ironmak. Steelmak.* **1993**, *20*, 35–41.
16. Pressouyre, G.M.; Bernstein, I.M. A quantitative analysis of hydrogen trapping. *Metall. Mater. Trans. A* **1978**, *9*, 1571–1580. [[CrossRef](#)]
17. DeArdo, A.J.; Hua, M.J.; Cho, K.G.; Garcia, C.I. On strength of microalloyed steels: An interpretive review. *Mater. Sci. Technol.* **2009**, *25*, 1074–1082. [[CrossRef](#)]
18. Vervynckt, S.; Verbeke, K.; Lopez, B.; Jonas, J.J. Modern HSLA steels and role of non-recrystallisation temperature. *Int. Mater. Rev.* **2012**, *57*, 187–207. [[CrossRef](#)]
19. Baker, T.N. Microalloyed Steels. *Ironmak. Steelmak.* **2016**, *4*, 264–307. [[CrossRef](#)]
20. DeArdo, A.J. *Microalloying '95*; ISS-AIME: Warrendale, PA, USA, 1995; Volume 15.
21. DeArdo, A.J. Niobium in Modern Steels. *Int. Mater. Rev.* **2003**, *48*, 371–402. [[CrossRef](#)]
22. Gilman, T. *The Physical Metallurgy of Microalloyed Steel*; Cambridge University Press: Cambridge, UK, 1957.
23. Baker, T.N. *Microalloyed Steel*; Future Developments of Metals and Ceramics; Institute of Materials: London, UK, 1992; pp. 75–119.
24. Gladman, T. *Microalloyed Steels*; Institute of Materials: London, UK, 1997.
25. Xie, K.Y.; Zheng, T.; Cairney, J.M.; Kaul, H.; Williams, J.G.; Barbaro, F.J.; Killmore, C.R.; Ringer, S.P. Strengthening from Nb-rich clusters in a Nb-microalloyed steel. *Scr. Mater.* **2012**, *66*, 710–713. [[CrossRef](#)]
26. Soto, R.; Saikaly, W.; Bano, X.; Issartel, C.; Rigaut, G.; Charai, A. Statistical and theoretical analysis of precipitates in dual-phase steels microalloyed with titanium and their effect on mechanical properties. *Acta Mater.* **1999**, *47*, 3475–3481. [[CrossRef](#)]
27. Mangonon, P.L., Jr.; Heitmann, W.E. *Proceeding Conference Microalloying*; Union Carbide Corporation: Houston, TX, USA, 18–21 November 1977.
28. Zhang, L.; Kannengiesser, T. Austenite grain growth and microstructure control in simulated heat affected zones of microalloyed HSLA steel. *Mater. Sci. Eng. A* **2014**, *613*, 326–335. [[CrossRef](#)]
29. Gu, Y.; Tian, P.; Wang, X.; Han, X.; Liao, B.; Xiao, F. Non-isothermal prior austenite grain growth of a high-Nb X100 pipeline steel during a simulated welding heat cycle process. *Mater. Des.* **2016**, *89*, 589–596. [[CrossRef](#)]
30. Karmakar, A.; Biswas, S.; Mukherjee, S.; Chakrabarti, D.; Kumar, V. Effect of composition and thermo-mechanical processing schedule on the microstructure, precipitation and strengthening of Nb-microalloyed steels. *Mater. Sci. Eng. A* **2017**, *690*, 158–169. [[CrossRef](#)]

31. Chen, G.; Yang, W.; Guo, S.; Sun, Z. Effect of Nb on the transformation kinetics of low carbon (manganese) steel during deformation of undercooled austenite. *J. Univ. Sci. Technol. Beijing Miner. Metall. Mater.* **2006**, *13*, 411–415. [[CrossRef](#)]
32. Baker, T.N. *Titanium Technology in Microalloyed Steels*, 2nd ed.; The Institute of Materials, Minerals and Mining: London, UK, 1997.
33. Kojima, A.; Yoshii, K.; Hada, T. Development of high HAZ toughness steel plates for box columns with high heat input welding. *Nippon Steel Tech. Rep.* **2004**, *90*, 39–44.
34. Chen, Y.; Zhang, D.T.; Liu, Y.C.; Li, H.J.; Xu, D.K. Effect of dissolution and precipitation of Nb on the formation of acicular ferrite/bainite ferrite in low-carbon HSLA steels. *Mater. Charact.* **2013**, *84*, 232–239. [[CrossRef](#)]
35. Karjalainen, L.P.; Maccagno, T.M.; Jonas, J.J. Softening and Flow Stress Behaviour of Nb Microalloyed Steels during Hot Rolling Simulation. *ISIJ Int.* **1995**, *35*, 1523–1531. [[CrossRef](#)]
36. Hansen, S.S.; Sande, J.B.V.; Cohen, M. Niobium Carbonitride Precipitation and Austenite Recrystallization in Hot-Rolled Microalloyed Steels. *Metall. Trans. A* **1987**, *11*, 387–402. [[CrossRef](#)]
37. He, X.L.; Shang, C.; Yang, S. *High Performance Low Carbon Bainitic Steel*; Metallurgical Industry Press: Beijing, China, 2008.
38. Hoogendoorn, T.M.; Spanraft, M.J. Quantifying the Effect of Microalloying Elements on Structures during Processing. In Proceedings of the International Symposium on High-Strength, Low-Alloy Steels, Washington, DC, USA, 1–3 October 1975.
39. LeBon, A.B.; de Saint-Martin, L.N. Using Laboratory Simulations to Improve Rolling Schedules and Equipment. In Proceedings of the International Symposium on High-Strength, Low-Alloy Steels, Washington, DC, USA, 1–3 October 1975.
40. Gauthier, G.; LeBon, A.B. Discussion: On the Recrystallization of Austenite. In Proceedings of the International Symposium on High-Strength, Low-Alloy Steels, Washington, DC, USA, 1–3 October 1975.
41. Gauthier, G.; LeBon, A.B. Discussion: Techniques of Assessment of Precipitation Kinetics. In Proceedings of the International Symposium on High-Strength, Low-Alloy Steels, Washington, DC, USA, 1–3 October 1975.
42. Tanaka, T.; Tabata, N.; Hatomura, T.; Shiga, C. Three Stages of the Controlled-Rolling Process. In Proceedings of the International Symposium on High-Strength, Low-Alloy Steels, Washington, DC, USA, 1–3 October 1975.
43. Kozasu, I.; Ouchi, C.; Sampei, T.; Okita, T. Hot Rolling as a High-Temperature Thermo-Mechanical Process. In Proceedings of the International Symposium on High-Strength, Low-Alloy Steels, Washington, DC, USA, 1–3 October 1975.
44. Gray, J.M.; Barbaro, F. Evolution of microalloyed steels since microalloying '75 with specific emphasis on linepipe and plate. In *HSLA Steels 2015, Microalloying 2015 & Offshore Engineering Steels 2015*; The Minerals, Metals & Materials Society: Pittsburgh, PA, USA, 2016; pp. 53–70.
45. Stalheim, D.G. The use of high temperature processing (HTP) steel for high strength oil and gas transmission pipeline application. *Iron Steel* **2005**, *40*, 699–704.
46. Bracke, L.; de Wispelaere, N.; Ahmed, H.; Gungor, O.E. S700MC/Grade 100 in heavy gauges: Industrialisation at ArcelorMittal europe. In Proceedings of the International Symposium on Recent Developments in Plate Steels, Warrendale, PA, USA, 19–22 June 2011; pp. 131–138.
47. Kim, S.J.; Lee, C.G.; Lee, T.H.; Lee, S. Effects of coiling temperature on microstructure and mechanical properties of high-strength hot-rolled steel plates containing Cu, Cr and Ni. *ISIJ Int.* **2000**, *40*, 692–698. [[CrossRef](#)]
48. Misra, R.D.K.; Nathani, H.; Hartmann, J.E.; Siciliano, F. Microstructural evolution in a new 770 MPa hot rolled Nb–Ti microalloyed steel. *Mater. Sci. Eng. A* **2005**, *394*, 339–352. [[CrossRef](#)]
49. Reip, C.P.; Shanmugam, S.; Misra, R.D.K. High strength microalloyed CMn (V–Nb–Ti) and CMn (V–Nb) pipeline steels processed through CSP thin-slab technology: Microstructure, precipitation and mechanical properties. *Mater. Sci. Eng. A* **2006**, *424*, 307–3017. [[CrossRef](#)]
50. Shanmugam, S.; Misra, R.D.K.; Hartmann, J.E.; Jansto, S.G. Microstructure of high strength niobium-containing pipeline steel. *Mater. Sci. Eng. A* **2006**, *441*, 215–229. [[CrossRef](#)]
51. Misra, R.D.K.; Jia, Z.; O'Malley, R.; Jansto, S.G. Precipitation behavior during thin slab thermomechanical processing and isothermal aging of copper-bearing niobium-microalloyed high strength structural steels: The effect on mechanical properties. *Mater. Sci. Eng. A* **2011**, *528*, 8772–8780. [[CrossRef](#)]

52. Riva, R.; Mapelli, C.; Venturini, R. Effect of Coiling Temperature on Formability and Mechanical Properties of Mild Low Carbon and HSLA Steels Processed by Thin Slab Casting and Direct Rolling. *ISIJ Int.* **2007**, *47*, 1204–1213. [[CrossRef](#)]
53. Misra, D.; Jansto, S.G. Niobium-based alloy design for structural applications. In *HSLA Steels 2015, Microalloying 2015 & Offshore Engineering Steels 2015*; The Minerals, Metals & Materials Society: Pittsburgh, PA, USA, 2016; pp. 261–266.
54. Challa, V.S.A.; Zhou, W.H.; Misra, R.D.K.; O'Malley, R.; Jansto, S.G. The effect of coiling temperature on the microstructure and mechanical properties of a niobium–titanium microalloyed steel processed via thin slab casting. *Mater. Sci. Eng. A* **2014**, *595*, 143–153. [[CrossRef](#)]
55. Maubane, R.; Banks, K.M.; Tuling, A.S. Hot strength during coiling of low C and Nb microalloyed steels. In *HSLA Steels 2015, Microalloying 2015 & Offshore Engineering Steels 2015*; The Minerals, Metals & Materials Society: Pittsburgh, PA, USA, 2016; pp. 323–328.
56. Burgmann, F.A.; Xie, Y.; Cairney, J.M.; Ringer, S.P.; Killmore, C.R.; Barbaro, F.J.; Williams, J.G. The effect of niobium additions on ferrite formation in Castrip[®] steel. *Mater. Forum* **2008**, *32*, 9–12.
57. Thelning, K.E. *Steel and Its Heat*; Butterworth & Co.: London, UK, 1984.
58. Song, R.; Ponge, D.; Raabe, D. Influence of Mn content on microstructure and mechanical properties of ultrafine grained C-Mn Steels. *ISIJ Int.* **2005**, *45*, 1721–1726. [[CrossRef](#)]
59. Shen, Y.F.; Zuo, L. High-strength low-alloy steel strengthened by multiply nanoscale microstructures. In *HSLA Steels 2015, Microalloying 2015 & Offshore Engineering Steels 2015*; The Minerals, Metals & Materials Society: Pittsburgh, PA, USA, 2016; pp. 187–193.
60. Hall, E.O. The deformation and ageing of mild steel: 3 discussion of results. *Proc. Phys. Soc.* **1951**, *64*, 747–753. [[CrossRef](#)]
61. Petch, N.J. The cleavage strength of polycrystals. *J. Iron Steel Inst.* **1953**, *174*, 25–28.
62. Sanz, L.; Pereda, B.; López, B. Effect of thermomechanical treatment and coiling temperature on the strengthening mechanisms of low carbon steels microalloyed with Nb. *Mater. Sci. Eng. A* **2017**, *685*, 377–390. [[CrossRef](#)]
63. Lucas, A.; Simon, P.; Bourdon, G.; Herman, J.C.; Riche, P.; Neutjens, J.; Harlet, P. Metallurgical Aspects of Ultra Fast Cooling in front of the Down-Coiler. *Steel Res. Int.* **2004**, *75*, 139–146. [[CrossRef](#)]
64. Mohapatra, S.S.; Ravikumar, S.V.; Pal, S.K.; Chakraborty, S. Ultra Fast Cooling of a Hot Steel Plate by Using High Mass Flux Air Atomized Spray. *Steel Res. Int.* **2013**, *84*, 229–236. [[CrossRef](#)]
65. Bhattacharya, P.; Samanta, A.N.; Chakraborty, S. Spray evaporative cooling to achieve Ultra Fast cooling in runout table. *Int. J. Therm. Sci.* **2009**, *48*, 1741–1747. [[CrossRef](#)]
66. Siciliano, F. High-Strength Linepipe Steels and Physical Simulation of Production Processes. In *Advanced High Strength Steel*; Springer: Singapore, 2018; pp. 71–78.
67. Gilman, T. *The Physical Metallurgy of Microalloyed Steel*; Cambridge University Press: Cambridge, UK, 1977.
68. Korchynsky, M. *Microalloying 75*; Union Carbide: New York, NY, USA, 1977.
69. DeArdo, A.J.; Ratz, G.A.; Wray, J.P. *Thermomechanical Processing of Microalloyed Austenite*; Metallurgical Society of AIME: Warrendale, PA, USA, 1982.
70. Korchynsky, M. (Ed.) *Proceedings of the HSLA—Technology and Applications: Conference Proceedings of International Conference on Technology and Applications of HSLA Steels*; American Society for Metals: Metals Park, OH, USA, 1983.
71. Taylor, K.A.; Thompson, S.W.; Fletcher, F.B. *Physical Metallurgy of Direct-Quenched Steels*; Minerals, Metals and Materials Society: Chicago, IL, USA, 1993.
72. Fazeli, F.; Amirkhiz, B.S.; Scott, C.; Arafin, M.; Collins, L. Kinetics and microstructural change of low-carbon bainite due to vanadium microalloying. *Mater. Sci. Eng. A* **2018**, *720*, 248–256. [[CrossRef](#)]
73. Gray, J.M. *An Independent View of Linepipe and Linepipe Steel for High Strength Pipelines: How to Get Pipe That's Right for the Job at the Right Price*; Microalloyed Steel Institute L.P.: Houston, TX, USA, 2002.
74. Tsunekage, N.; Kobayashi, K.; Tsubakino, H. Influence of S and V on toughness of ferrite-pearlite or bainite steels. *Curr. Adv. Mater. Processes* **2000**, *13*, 534.
75. Nomura, I. Metallurgical Technology in Microalloyed Steels for Automotive Parts. *Mater. Jpn.* **1995**, *34*, 705. [[CrossRef](#)]
76. Tomita, Y.; Saito, N.; Tsuzuki, T.; Tokunaga, Y.; Okamoto, K. Improvement in HAZ Toughness of Steel by TiN-MnS Addition. *ISIJ Int.* **1994**, *34*, 829–835. [[CrossRef](#)]

77. Suzuki, S.; Kuroki, K.; Kobayashi, H.; Takahashi, N. Sn Segregation at Grain Boundary and Interface between MnS and Matrix in Fe-3 mass%Si Alloys Doped with Tin. *Mater. Trans. JIM* **1992**, *33*, 1068–1076. [[CrossRef](#)]
78. Tsunekage, N.; Tsubakino, H. Effects of Sulfur Content and Sulfide-forming Elements Addition on Impact Properties of Ferrite–Pearlitic Microalloyed Steels. *ISIJ Int.* **2001**, *41*, 498–505. [[CrossRef](#)]
79. DeArdo, A.J. Microalloyed Steels: Past, Present and Future. In *HSLA Steels 2015, Microalloying 2015 and Offshore Engineering Steels, 2015*; The Minerals, Metals & Materials Society: Pittsburgh, PA, USA, 2015.
80. Cottrell, A.H. *Dislocations and Plastic Flow in Crystals*; Clarendon Press: Oxford, UK, 1964.
81. Korchynsky, M. Microalloyed Steels. In *Proc. Conf. Microalloying '75*; Union Carbide Corp.: New York, NY, USA, 1977.
82. Bai, D.; Collins, L.; Hamad, F.; Chen, X.; Klein, R. Microstructure and mechanical properties of high strength linepipes steels. In *Proceedings of the Materials. Science & Technology Congress*; AIST/ASM: Warrendale, PA, USA, 2007; pp. 355–366.
83. Peters, P.A.; Gray, J.M. *Genesis and Development of Specifications and Performance Requirements for Modern Linepipe—Strength, Toughness, Corrosion Resistance and Weldability*; International Convention; Australian Pipeline Industry Association, Inc.: Hobart, Tasmania, Australia, 24–29 October 1992.
84. Siwecki, T.; Eliasson, J.; Lagneborg, R.; Hutchinson, B. Vanadium microalloyed bainitic hot strip steels. *ISIJ Int.* **2010**, *50*, 760–767. [[CrossRef](#)]
85. Kim, Y.W.; Song, S.W.; Seo, S.J.; Hong, S.G.; Lee, C.S. Development of Ti and Mo micro-alloyed hot-rolled high strength sheet steel by controlling thermomechanical controlled processing schedule. *Mater. Sci. Eng. A* **2013**, *565*, 430–438. [[CrossRef](#)]
86. Juanhua, K.; Lin, Z.; Bin, G.; Pinghe, L.; Aihua, W.; Changsheng, X. Influence of Mo content on microstructures and mechanical properties of high strength pipeline steel. *Mater. Des.* **2004**, *25*, 723–728. [[CrossRef](#)]
87. Xiao, F.R.; Liao, B.; Shan, Y.Y.; Qiao, G.Y.; Zhong, Y.; Zhang, C.; Yang, K. Challenge of mechanical properties of an acicular ferrite pipeline steel. *Mater. Sci. Eng. A* **2006**, *431*, 41–52. [[CrossRef](#)]
88. Wang, W.; Shan, Y.; Yang, K. Study of high strength pipeline steels with different microstructures. *Mater. Sci. Eng. A* **2009**, *502*, 38–44. [[CrossRef](#)]
89. Katsumata, M.; Machida, M.; Kaji, H. Recrystallization of Austenite in High-Temperature Hot-Rolling of Niobium Bearing Steels. In *Proceedings of the International Conference on the Thermomechanical Austenite*, Pittsburgh, PA, USA, 17–19 August 1981.
90. Suikkanen, P.P.; Komi, J.I.; Karjalainen, L.P. Effect of austenite deformation and chemical composition on the microstructure and hardness of low-carbon and ultra low-carbon bainitic steels. *Met. Sci. Heat Treat.* **2005**, *47*, 507–511. [[CrossRef](#)]
91. Gong, P.; Palmiere, E.J.; Rainforth, W.M. Thermomechanical processing route to achieve ultrafine grains in low carbon microalloyed steels. *Acta Mater.* **2016**, *119*, 43–54. [[CrossRef](#)]
92. Dutta, B.; Valdes, E.; Sellars, C.M. Mechanism and kinetics of strain induced precipitation of Nb (C, N) in austenite. *Acta Mater.* **1992**, *40*, 653–662. [[CrossRef](#)]
93. Gomez, M.; Valles, P.; Medina, S.F. Evolution of microstructure and precipitation state during thermomechanical processing of a X80 microalloyed steel. *Mater. Sci. Eng. A* **2011**, *528*, 4761–4773. [[CrossRef](#)]
94. Zhao, M.C.; Yang, K.; Shan, Y. The effects of thermo-mechanical control process on microstructures and mechanical properties of a commercial pipeline steel. *Mater. Sci. Eng. A* **2002**, *335*, 14–20. [[CrossRef](#)]
95. Zhao, M.C.; Yang, K.; Shan, Y.Y. Comparison on strength and toughness behaviors of microalloyed pipeline steels with acicular ferrite and ultrafine ferrite. *Mater. Lett.* **2003**, *57*, 1496–1500. [[CrossRef](#)]
96. Xu, Y.B.; Yu, Y.M.; Xiao, B.L.; Liu, Z.Y.; Wang, G.D. Microstructural evolution in an ultralow-C and high-Nb bearing steel during continuous cooling. *J. Mater. Sci.* **2009**, *44*, 3928–3935. [[CrossRef](#)]
97. Graf, M.K.; Hillenbrand, H.; Peters, P. *Accelerated Cooling of Steel*; TMS-AIME: Warrendale, PA, USA, 1986; pp. 165–179.
98. Xiang-dong, H.; Lie-jun, L.; Zheng-wu, P.; Song-jun, C. Effects of TMCP schedule on precipitation, microstructure and properties of Ti-microalloyed high strength steel. *J. Iron Steel Res. Int.* **2016**, *23*, 593–601.
99. Jorge, J.C.F.; Souza, L.F.G.; Rebello, J.M.A. The effect of chromium on the microstructure/toughness relationship of C-Mn weld metal deposits. *Mater. Charact.* **2001**, *47*, 195–205. [[CrossRef](#)]
100. Beidokhti, B.; Koukabi, A.H.; Dolati, A. Influences of titanium and manganese on high strength low alloy SAW weld metal properties. *Mater. Charact.* **2009**, *60*, 225–233. [[CrossRef](#)]

101. Dongsheng, L.; Binggui, C.; Yuanyan, C. Strengthening and Toughening of a Heavy Plate Steel for Shipbuilding with Yield Strength of Approximately 690 MPa. *Metall. Mater. Trans. A* **2013**, *44*, 440–445.
102. Shin, S.Y.; Han, S.Y.; Hwang, B.C.; Lee, C.G.; Lee, S.H. Effects of Cu and B addition on microstructure and mechanical properties of high-strength bainitic steels. *Mater. Sci. Eng. A* **2009**, *517*, 212–218. [[CrossRef](#)]
103. Han, S.Y.; Shin, S.Y.; Lee, S.H.; Kim, N.J.; Bae, J.H.; Kim, K. Effects of Cooling Conditions on Tensile and Charpy Impact Properties of API X80 Linepipe Steels. *Metall. Mater. Trans. A* **2010**, *41*, 329–340. [[CrossRef](#)]
104. Kang, Y.L.; Han, Q.H.; Zhao, X.M.; Cai, M.H. Influence of nanoparticle reinforcements on the strengthening mechanism of an ultrafine-grained dual phase steel containing titanium. *Mater. Des.* **2013**, *44*, 331–339. [[CrossRef](#)]
105. Wang, Y.W.; Feng, C.; Xu, F.Y.; Bai, B.Z.; Fang, H.Z. Influence of Nb on Microstructure and Property of Low-Carbon Mn-Series Air-Cooled Bainitic Steel. *J. Iron Steel Res. Int.* **2010**, *17*, 49–53. [[CrossRef](#)]
106. Kong, J.H.; Xie, C.S. Effect of molybdenum on continuous cooling bainite transformation of low-carbon microalloyed Steel. *Mater. Des.* **2006**, *27*, 1169–1173. [[CrossRef](#)]
107. Zackay, V.F.; Justusson, W.M. *Special Report 76*; Iron and Steel Institute: London, UK, 1962.
108. Hara, T.; Asahi, H.; Uemori, R.; Tamehiro, H. Role of combined addition of niobium and boron and of molybdenum and boron on hardenability in low carbon steels. *ISIJ Int.* **2004**, *44*, 1431–1440. [[CrossRef](#)]
109. Luo, H.; Karjalainen, L.P.; Porter, D.A.; Liimatainen, H.M.; Zhang, Y. The influence of Ti on the hot ductility of Nb-bearing steels in simulated continuous casting process. *ISIJ Int.* **2002**, *42*, 273–282. [[CrossRef](#)]
110. Shukla, R.; Das, S.K.; Kumar, B.R.; Ghosh, S.K.; Kundu, S.; Chatterjee, S. An Ultra-low Carbon, Thermomechanically Controlled Processed Microalloyed Steel: Microstructure and Mechanical Properties. *Metall. Mater. Trans. A* **2012**, *43*, 4835–4845. [[CrossRef](#)]
111. Li, C.N.; Ji, F.Q.; Yua, G.; Kang, J.; Misra, R.D.K.; Wang, G.D. The impact of thermos-mechanical controlled processing on structure-property relationship and strain hardening behavior in dual-phase steels. *Mater. Sci. Eng. A* **2016**, *662*, 100–110. [[CrossRef](#)]
112. Oliver, S.; Jones, T.B.; Fournalis, G. Dual phase versus TRIP strip steels: Microstructural changes as a consequence of quasi-static and dynamic tensile testing. *Mater. Charact.* **2007**, *58*, 390–400. [[CrossRef](#)]
113. Li, X.L.; Lei, C.S.; Deng, X.T.; Wang, Z.D.; Yu, Y.G.; Wang, G.D.; Misra, R.D.K. Precipitation strengthening in titanium microalloyed high-strength steel plates with new generation-thermomechanical controlled processing (NG-TMCP). *J. Alloys Compd.* **2016**, *689*, 542–553. [[CrossRef](#)]
114. Zhao, M.C.; Yang, K.; Xiao, F.R.; Shan, Y.Y. Continuous cooling transformation of undeformed and deformed low carbon pipeline steels. *Mater. Sci. Eng. A* **2003**, *355*, 126–136. [[CrossRef](#)]
115. Bose-Filho, W.W.; Carvalho, A.L.M.; Strangw, M. Effects of alloying elements on the microstructure and inclusion formation in HSLA multipass welds. *Mater. Charact.* **2007**, *58*, 29–39. [[CrossRef](#)]
116. Beidokhti, B.; Kokabi, A.H.; Dolati, A. A comprehensive study on the microstructure of high strength low alloy pipeline welds. *J. Alloys Compd.* **2014**, *597*, 142–147. [[CrossRef](#)]
117. Bailey, N.; Jones, S.B. *Solidification Cracking of Ferritic Steel during Submerged Arc-Welding*; Welding Institute: Cambridge, UK, 1978; pp. 217–231.
118. Mandelberg, S.L.; Rybacov, A.A.; Sidorenko, B.G. Resistance of pipe steel welded joints to solidification cracks. *Avtom. Svarka* **1972**, *3*, 1–5.
119. Shiga, C. Effects of steelmaking, alloying and rolling variables on the HAZ structure and properties in microalloyed plate and line pipe. In Proceedings of the International Conference on The Metallurgy, Welding, and Qualification of Microalloyed (HSLA) Steel Weldments, Houston, TX, USA, 6–8 November 1990; pp. 327–350.
120. Aihara, S.; Okamoto, K. Influence of Local Brittle Zone on HAZ Toughness of TMCP Steels. In Proceedings of the International Conference on The Metallurgy, Welding, and Qualification of Microalloyed (HSLA) Steel Weldments, Houston, TX, USA, 6–8 November 1990; pp. 402–426.
121. García, R.; López, V.H.; Lazaro, Y.; Aguilera, J. *Grain Refinement in Electrodeposited Microalloyed Steels by Inducing a Centred Magnetic Field*; Soldagem & Inspecao: Sao Paulo, Brasil, 2007; pp. 300–304.
122. Loberg, B.; Nordgren, A.; Strid, J.; Easterling, K.E. The Role of Alloy Composition on the Stability of Nitrides in Ti-Microalloyed Steels during Weld Thermal Cycles. *Metall. Trans. A* **1984**, *15*, 33–41. [[CrossRef](#)]
123. Zhang, W.; Elmer, J.W.; DebRoy, T. Modeling and real time mapping of phases during GTA welding of 1005 steel. *Mater. Sci. Eng. A* **2002**, *333*, 320–335. [[CrossRef](#)]

124. Wan, X.L.; Wang, H.H.; Cheng, L.; Wu, K.M. The formation mechanisms of interlocked microstructures in low-carbon high-strength steel weld metals. *Mater. Charact.* **2012**, *67*, 41–51. [[CrossRef](#)]
125. Terada, Y.; Tamehiro, H.; Morimoto, H.; Hara, T.; Tsuru, E.; Asahi, H. X100 Linepipe With Excellent HAZ Toughness and Deformability. In Proceedings of the 22nd International Conference on Offshore Mechanics and Arctic Engineering ASME, Cancun, Mexico, 8–13 June 2003; pp. 1–8.
126. Matsuda, F.; Ikeuchi, K.; Liao, J.S.; Tanabe, H. Weld HAZ Toughness and Its Improvement of Low Alloy Steel SQV-2A for Pressure Vessels (Report 2): Microstructure and Charpy Impact Behavior of Intercritically Reheated Coarse Grained Heat Affected Zone (ICCGHAZ) (Materials, Metallurgy & Weldability). *Trans. JWRI* **1994**, *23*, 49–57.
127. Shim, J.H.; Cho, Y.W.; Chung, S.H.; Shim, J.D.; Lee, D.N. Nucleation of intragranular ferrite at Ti_2O_3 particle in low carbon steel. *Acta Mater.* **1999**, *47*, 2751–2760. [[CrossRef](#)]
128. Guo, A.M.; Li, S.R.; Guo, J.; Li, P.H.; Ding, Q.F.; Wu, K.M.; He, X.L. Effect of zirconium addition on the impact toughness of the heat affected zone in a high strength low alloy pipeline steel. *Mater. Charact.* **2008**, *59*, 134–139. [[CrossRef](#)]
129. Lee, J.L.; Pan, Y.T. The Formation of Intragranular Acicular Ferrite in Simulated Heat-affected Zone. *ISIJ Int.* **1995**, *35*, 1027–1033. [[CrossRef](#)]
130. Gianetto, J.A.; Braid, J.E.M.; Bowker, J.T.; Tyson, W.R. Heat-Affected Zone Toughness of a TMCP Steel Designed for Low-Temperature Applications. *Trans. ASME* **1997**, *119*, 134–144. [[CrossRef](#)]
131. Matsuda, F.; Ikeuchi, K.; Fukada, Y.; Horii, Y.; Okada, H.; Shiwaku, T.; Shiga, C.; Suzuki, S. Review of Mechanical and Metallurgical Investigations of M-A Constituent in Welded Joint in Japan. *Trans. JWRI* **1995**, *24*, 1–24.
132. Lan, L.; Qiu, C.; Zhao, D.; Gao, X.; Du, L. Microstructural characteristics and toughness of the simulated coarse grained heat affected zone of high strength low carbon bainitic steel. *Mater. Sci. Eng. A* **2011**, *529*, 192–200. [[CrossRef](#)]
133. Hunt, A.C.; Kluken, A.O.; Edwards, G.R. Heat input and dilution effects in microalloyed steel weld metals. *Weld. J.* **1994**, *73*, 9–15.
134. Karabulut, H.; Türkmen, M.; Erden, M.A.; Gündüz, S. Effect of Different Current Values on Microstructure and Mechanical Properties of Microalloyed Steels Joined by the Submerged Arc Welding Method. *Metals* **2016**, *6*, 281. [[CrossRef](#)]
135. Zhang, W.; Elmer, J.W.; DebRoy, T. Kinetics of ferrite to austenite transformation during welding of 1005 steel. *Scr. Mater.* **2002**, *46*, 753–757. [[CrossRef](#)]
136. Ekicia, M.; Ozsarac, U. Investigation of Mechanical Properties of Microalloyed Steels Joined by GMAW and Electrical Arc Welding. *Acta Phys. Pol. A* **2013**, *123*, 289–290. [[CrossRef](#)]
137. Dunder, M.; Vuherer, T.; Samardžić, I. Weldability of microalloyed high strength steels TStE 420 and S960QL. *Metallurgija* **2014**, *53*, 335–338.
138. Sharma, V.; Shahi, A.S. Quenched and tempered steel welded with micro-alloyed based ferritic fillers. *J. Mater. Process. Technol.* **2018**, *253*, 2–16. [[CrossRef](#)]
139. Liu, H.J.; Shen, J.J.; Zhou, L.; Zhao, Y.Q.; Li, C. Microstructural characterisation and mechanical properties of friction stir welded joints of aluminium alloy to copper. *Sci. Technol. Weld. Join.* **2011**, *16*, 92–99. [[CrossRef](#)]
140. Hart, P.H.M.; Harrison, P.L. Compositional Parameters for HAZ Cracking and Hardening in C-Mn Steels. In Proceedings of the 67th Annual AWS Meeting, Atlanta, GA, USA, 14–16 April 1986; pp. 13–18.
141. Wang, S.H.; Luu, W.C.; Ho, K.F.; Wu, J.K. Hydrogen permeation in a submerged arc weldment of TMCP steel. *Mater. Chem. Phys.* **2002**, *77*, 447–454. [[CrossRef](#)]
142. Sun, Q.; Di, H.; Li, J.; Wu, B.; Misra, R. A comparative study of the microstructure and properties of 800 MPa microalloyed C-Mn steel weld joints by laser and gas metal arc welding. *Mater Sci Eng A* **2016**, *669*, 150–158. [[CrossRef](#)]
143. Wang, X.; Zhang, S.; Zhou, J.; Zhang, M.; Chen, C.; Misra, R. Effect of heat input on microstructure and properties of hybrid fiber laser-arc weld joints of the 800 MPa hot-rolled Nb-Ti-Mo microalloyed steels. *Opt. Lasers Eng.* **2017**, *91*, 86–96. [[CrossRef](#)]
144. Zhang, M.; Wang, X.; Zhu, G.; Chen, C.; Hou, J.; Zhang, S.; Jing, H. Effect of laser welding process parameters on microstructure and mechanical properties on butt joint of new hot-rolled nano-scale precipitate strengthen steel. *Acta Metall. Sin.* **2014**, *27*, 521–529. [[CrossRef](#)]
145. Bhadesia, H. *Bainite in Steels*; The Institute of Materials: London, UK, 1992.

146. Pamnani, R.; Karthik, V.; Jayamukar, T.; Vasudevan, M.; Sakthivel, T. Evaluation of Mechanical Properties across Micro Alloyed HSLA Steel Weld Joints using Atomated Ball Indentation. *Mater. Sci. Eng. A* **2015**, *651*, 214–223. [[CrossRef](#)]
147. Chatzidouros, E.V.; Papazoglou, V.J.; Tsiourva, T.E.; Pantelis, D.I. Hydrogen effect on fracture toughness of pipeline steel welds, with insitu hydrogen charging. *Int. J. Hydrog. Energy* **2011**, *36*, 12626–12643. [[CrossRef](#)]
148. Demofonti, G.; Mannucci, G.; Di Biagio, M.; Hillenbrand, H.G.; Harris, D. Fracture propagation resistance evaluation of X100 TMCP steel pipes for high pressure gas transportation pipelines by full scale burst tests. *Pipeline Technol. Proc.* **2004**, *1*, 467–482.
149. Yakubtsov, I.A.; Poruks, P.; Boyd, J.D. Microstructure and mechanical properties of bainitic low carbon high strength plate steels. *Mater. Sci. Eng. A* **2008**, *480*, 109–116. [[CrossRef](#)]
150. Woodtli, J.; Kieselbach, R. Damage due to hydrogen embrittlement and stress corrosion cracking. *Eng. Fail. Anal.* **2000**, *7*, 427–450. [[CrossRef](#)]
151. Hui, W.J.; Weng, Y.Q.; Dong, H. *Steels for High Strength Fastener*; Metallurgical Industry Press: Beijing, China, 2009.
152. Cottis, R.A. *Hydrogen Embrittlement*; School of Materials: Manchester, UK, 2010.
153. Domizzi, G.; Anteri, G.; Ovejero-García, J. Influence of sulphur content and inclusion distribution on the hydrogen induced blister cracking in pressure vessel and pipeline steels. *Corros. Sci.* **2001**, *43*, 325–339. [[CrossRef](#)]
154. Hardie, D.; Charles, E.A.; Lopez, A.H. Hydrogen embrittlement of high strength pipeline steels. *Corros. Sci.* **2006**, *48*, 4378–4385. [[CrossRef](#)]
155. Shin, S.Y.; Hwang, B.; Lee, S.; Kim, N.J.; Ahn, S.S. Correlation of microstructure and charpy impact properties in API X70 and X80 line-pipe steels. *Mater. Sci. Eng. A* **2007**, *458*, 281–289. [[CrossRef](#)]
156. Shterenlikht, A.; Hashemi, S.H.; Howard, I.C.; Yates, J.R.; Andrews, R.M. A specimen for studying the resistance to ductile crack propagation in pipes. *Eng. Fract. Mech.* **2004**, *71*, 1997–2013. [[CrossRef](#)]
157. Asoaka, T.; Lapasset, G.; Aucouturier, M.; Lacombe, P. Observation of hydrogen trapping in Fe-0.15 wt % Ti alloy by high resolution autoradiography. *Corrosion* **1978**, *34*, 39–47. [[CrossRef](#)]
158. Qian, L.; Andrej, A. Reversible hydrogen trapping in a 3.5 NiCrMoV medium strength steel. *Corros. Sci.* **2015**, *96*, 112–120.
159. Mohsen, D.; Martin, M.L.; Nagao, A.; Sofronis, P.; Robertson, I.M. Modeling hydrogen transport by dislocations. *J. Mech. Phys. Solids* **2015**, *78*, 511–525.
160. Marchetti, L.; Herms, E.; Lagoutaris, P.J. Hydrogen embrittlement susceptibility of tempered 9% Cr, 1% Mo steel. *Int. J. Hydrog. Energy* **2011**, *34*, 15880–15887. [[CrossRef](#)]
161. Druce, P.D.; Daniel, H.; Ahmed, A.S.; Aysha, J.H.; Andrzej, C.; Pereloma, V.E. Investigation of the effect of electrolytic hydrogen charging of x70 steel: I. The effect of microstructure on hydrogen-induced cold cracking and blistering. *Int. J. Hydrog. Energy* **2016**, *41*, 12411–12423.
162. Liu, Q.; Venezuela, J.; Zhang, M.; Zhou, Q.; Atrens, A. Hydrogen trapping in some advanced high strength Steels. *Corros. Sci.* **2016**, *111*, 770–785. [[CrossRef](#)]
163. Hirth, J. Effects of hydrogen on the properties of iron and steel. *Metall. Trans. A* **1980**, *11*, 861–890. [[CrossRef](#)]
164. Thomas, R.L.S.; Li, D.; Gangloff, R.P.; Scully, J.R. Trap-governed hydrogen diffusivity and uptake capacity in ultrahigh-strength AERMET 100 steel. *Metall. Mater. Trans. A* **2002**, *33*, 1991–2004. [[CrossRef](#)]
165. Venezuela, J.; Liu, Q.; Zhang, M.; Zhou, Q.; Atrens, A. The influence of hydrogen on the mechanical and fracture properties of some martensitic advanced high strength steels studied using the linearly increasing stress test. *Corros. Sci.* **2015**, *99*, 98–117. [[CrossRef](#)]
166. Wei, F.G.; Tsuzaki, K. Quantitative analysis on hydrogen trapping of TiC particles in steel. *Metall. Mater. Trans. A* **2006**, *37*, 331–353. [[CrossRef](#)]
167. Depover, T.; Escobar, D.P.; Wallaert, E.; Zermout, Z.; Verbeken, K. Effect of hydrogen charging on the mechanical properties of advanced high strength steels. *Int. J. Hydrog Energy* **2014**, *39*, 4647–4656. [[CrossRef](#)]
168. Wallaert, E.; Depover, T.; Arafin, M.; Verbeken, K. Thermal desorption spectroscopy evaluation of the hydrogen-trapping capacity of NbC and NbN precipitates. *Metall. Mater. Trans. A* **2014**, *45*, 2412–2420. [[CrossRef](#)]
169. Takahashi, J.; Kawakami, K.; Kobayashi, Y.; Tarui, T. The first direct observation of hydrogen trapping sites in TiC precipitation-hardening steel through atom probe tomography. *Scr. Mater.* **2010**, *63*, 261–264. [[CrossRef](#)]

170. Valentini, R.; Solina, A.; Matera, S.; de Gregorio, P. Influence of titanium and carbon contents on the hydrogen trapping of microalloyed steels. *Metall. Mater.* **1996**, *27*, 3773–3780. [[CrossRef](#)]
171. McNabb, A.; Foster, P.K. A new analysis of the diffusion of hydrogen in iron and ferritic steels. *Trans. Metall. Soc. AIME* **1963**, *227*, 618–627.
172. Gangloff, R.P. *Hydrogen Assisted Cracking of High Strength Alloys*; In *Comprehensive Structural Integrity*; Elsevier: New York, NY, USA, 2003; pp. 31–101.
173. Lynch, S. Hydrogen embrittlement phenomena and mechanisms. *Corros. Rev.* **2012**, *30*, 105–123. [[CrossRef](#)]
174. Oriani, R.A. A mechanistic theory of hydrogen embrittlement of steels. *Berich. Bunsengesellsch. Phys. Chem.* **1972**, *76*, 848–857.
175. Beachem, C.D. A new model for hydrogen assisted cracking (Hydrogen embrittlement). *Metall. Trans. A* **1972**, *3*, 437–451. [[CrossRef](#)]
176. Lynch, S.P. Environmentally assisted cracking: Overview of evidence for an adsorption-induced localized-slip process. *Acta Metall.* **1988**, *20*, 2639–2661. [[CrossRef](#)]
177. Tehemiro, H.; Takeda, T.; Matsuda, S.; Yamamoto, K.; Komura, H. Effect of accelerated cooling after controlled rolling on the hydrogen-induced cracking resistance of pipeline steels. *Trans. Iron Steel Inst. Jpn.* **1985**, *25*, 982–988.
178. Ejim, F. Hydrogen Diffusion in Pipeline Steels. Ph.D. Thesis, Dipartimento di Chimica, Materiali e Ingegneria Chimica “Giulio Natta”, Milan, Italy, 2011.
179. Pasco, R.W.; Ficalora, P.J. *Hydrogen Degradation of Ferrous Alloys*; Noyes Publications: Park Ridge, NJ, USA, 1984; pp. 199–214.
180. Afrooz, B. *Hydrogen Embrittlement*; Saarland University: Saarbrücken, Germany, 2011.
181. Myers, S.M.; Baskes, M.L.; Brinbaum, H.K.; Corbett, J.W.; Deleo, G.G.; Estreicher, S.K.; Haller, E.E.; Jena, P.; Johnson, N.M.; Kirchheim, R.; et al. Hydrogen interactions with defects in crystalline solids. *Rev. Mod. Phys.* **1992**, *64*, 559. [[CrossRef](#)]
182. Xu, K. *Hydrogen Embrittlement of Carbon Steels and Their Welds*; Gaseous Hydrogen Embrittlement of Materials in Energy Technology; Woodhead: Philadelphia, IL, USA, 2012; pp. 526–561.
183. Walter, R.J.; Chandler, W.T. *Effects of High Pressure Hydrogen on Metals at Ambient Temperature*; No. N-70-18637; NASA-CR-102425; Rocketdyne: Canoga Park, CA, USA, 1968.
184. Thompson, A.W.; Bernstein, I.M. Selection of structural materials for hydrogen pipelines and storage vessels. *Int. J. Hydrog. Energy*, **1977**, *2*, 163–173. [[CrossRef](#)]
185. Imbihl, R.; Behm, R.J.; Christmann, K.; Ertl, G.; Matsushima, T. Phase transitions of a two-dimensional chemisorbed system: H on Fe(110). *Surface Sci.* **1982**, *117*, 257–266. [[CrossRef](#)]
186. Shanmugan, S.; Ramisetti, N.K.; Mirsa, R.D.K. Microstructure and High Strength-Toughness Combination of a New 700 MPa Nb Microalloyed Pipeline Steel. *Mater. Sci. Eng.* **2008**, *478*, 26–37. [[CrossRef](#)]
187. Liu, D.; Xu, H.; Yang, K.; Fang, H. Effect of bainite/Martensite Mixed Microstructure on the strength and toughness of low carbon alloy steels. *Acta Metall. Sin.* **2004**, *40*, 882–886.
188. Nayak, S.S.; Misra, R.D.K.; Hartmann, J.; Siciliano, F.; Gray, J.M. Microstructure and properties of low manganese and niobium containing HIC pipeline Steel. *Mater. Sci. Eng. A* **2008**, *494*, 456–463. [[CrossRef](#)]
189. Uranga, P.; Fernandez, A.I.; Lopez, B.; Rodriguez-Ibabe, J.M. Transition between static and metadynamic recrystallization kinetics in coarse Nb microalloyed austenite. *Mater. Sci. Eng. A* **2003**, *345*, 319–327. [[CrossRef](#)]
190. Zhou, M.; Du, L.X.; Liu, X.H. Relationship among Microstructure and properties and heat treatment of Ultra-High Strength X120 pipeline steel. *J. Iron Steel Res. Int.* **2011**, *18*, 59–64. [[CrossRef](#)]
191. Ping, Z. Microstructure and Mechanical Properties in Isothermal Tempering of High Co-Ni Secondary Hardening Ultrahigh Strength Steel. *Sch. Mater. Sci. Eng. Beijing* **2007**, *14*, 292–295.
192. Asahi, H.; Ueneo, M.; Yonezawa, T. Prediction of Sulfide Stress Cracking in High Strength Tubulars. *Corrosion* **1994**, *50*, 537. [[CrossRef](#)]
193. Lunarska, E.; Zielinski, A. *Hydrogen Degradation of Ferrous Alloys*; Noyes Publications: Park Ridge, NJ, USA, 1985.
194. Park, G.T.; Koh, S.U.; Jung, H.G.; Kim, K.Y. Effect of microstructure on the hydrogen trapping Efficiency induced Cracking of linepipe Steel. *Corros. Sci.* **2008**, *50*, 1865–1871. [[CrossRef](#)]
195. Liu, D.; Bai, B.; Fang, H.; Zhang, W.; Gu, J.; Chang, K. Effect of tempering and Carbide Free Bainite on the Mechanical Characteristics of a High Strength Low Alloy Steel. *Mater. Sci. Eng.* **2004**, *371*, 40–44. [[CrossRef](#)]

196. Dong, C.F.; Xiao, K.; Liu, Z.Y.; Yang, W.J.; Li, X.G. Hydrogen Induced Cracking of X80 pipeline Steel. *Int. J. Miner. Metall. Mater.* **2010**, *17*, 579–586. [[CrossRef](#)]
197. Das, A.K. The Present and the Future of Line Pipe Steels for Petroleum Industry. *Mater. Manuf. Processes* **2010**, *25*, 1–3. [[CrossRef](#)]
198. Meimeth, S.; Grimpe, F.; Meuser, H.; Siegel, H.; Stallybrass, C.; Heckmann, C.J. Development, state of the art and future trends in design and production of heavy plates in X80 steel-grades, steel rolling 2006. In Proceedings of the 9th International & 4th European Conferences, Paris, France, 19–21 June 2006.
199. Madías, J. *Nuevas Plantas Latinoamericanas; Industria del Acero: San Nicolás, Argentina*, 2017; pp. 28–43.
200. Jansto, S. Current development in niobium high carbon applications. In Proceedings of the MS&T 2011, Materials Science & Technology 2011 Conference and Exhibition (MS&T Partner Societies), Columbus, OH, USA, 16–20 October 2011.
201. Jansto, S. Applied metallurgy of the microniobium R alloy approach in long and plate products. In Proceedings of the METAL, Brno, Czech Republic, 23–25 May 2012.
202. Jansto, S. Metallurgical mechanism and niobium effects on improved mechanical properties in high carbon steels. In Proceedings of the Microalloying 2015 & O shore Engineering Steels 2015, Hangzhou, China, 11–13 November 2015; pp. 981–986.



© 2018 by the authors. Licensee MDPI, Basel, Switzerland. This article is an open access article distributed under the terms and conditions of the Creative Commons Attribution (CC BY) license (<http://creativecommons.org/licenses/by/4.0/>).